Project No. 01-59

PROPOSED ENHANCEMENTS TO PAVEMENT ME DESIGN: IMPROVED CONSIDERATION OF THE INFLUENCE OF SUBGRADE SOILS SUSCEPTIBLE TO SHRINK/SWELL AND/OR FROST HEAVE ON PAVEMENT PERFORMANCE

APPENDIX 1

THEORY AND LITERATURE REVIEW

MAY 2023

TABLE OF CONTENTS

LIST OF FIGURES

LIST OF TABLES

1. Input Soil Parameter Hierarchical Levels

This document summarizes the theory and literature review for subjects pertaining to shrink/swell (SS) soils, frost heave (FH) soils, pavement design when SS and/or FH soils are present, and statistical analyses for engineering practice.

1.1 Summary

Current engineering practice for determining the volume change behavior of unsaturated soils, including expansive and frost susceptible soils, are mostly based on simplified tests, correlations with index properties, or other empirical methods. Such practices, although useful for practical applications, can lead to poor and often uneconomical designs. As a result, distresses to foundations, pavements, and other structures on high volume change soils are common and repairing them can be quite expensive. Although the fundamental behavior of high-volume change soils under various soil compositional and environmental factors is not completely understood, there have been studies on engineering behavior and characterization practices of these soils that allows for better implementation techniques into current pavement design practice.

Under this task, the research team conducted an extensive literature review and collected information relevant to the existing models to predict the influence of shrink/swell and/or frost heave on pavement performance. The comprehensive review includes current and most updated mechanistic and empirical models available to predict high volume change behavior and frost heave of such soils. The literature presented was selected by considering the readiness of the implementation into the current Pavement ME Design guide; and it is expected that more information will be added as it becomes available during the development of Phase II of the project.

1.2 Objectives

The following objectives were completed as part of this study:

1. Review of unsaturated soil mechanics related to SS soils including theory, testing, and recent research advancements.
2. Review of FH soil mechanics including theory, testing, and recent research advancements
3. Review of statistical theory and Bayesian statistics

1.3 Stress States of Unsaturated Soils

Soils prone to volume change due to changes in water content are by nature, unsaturated; and their stress state conditions are different from those soils that are saturated. The stress state of a saturated soil was defined by Terzaghi in terms of effective stress,

$$\left[\sigma'\right] = \begin{bmatrix} (\sigma_x - u_w) & \tau_{yx} & \tau_{zx} \\ \tau_{xy} & (\sigma_y - u_w) & \tau_{zy} \\ \tau_{xz} & \tau_{yz} & (\sigma_z - u_w) \end{bmatrix}$$

where:
σ'is the effective normal stress; and σ_x, σ_y, σ_z are the total normal stresses in x, y, and z directions, respectively.

The effective stress principle has proven to be invaluable to the engineer who is concerned with the prediction of soil behavior. When the soil is saturated, the pore water pressure (u_w) is easily defined but, when the soil is not saturated, the water and air occupy the pore space and a different formulation is needed to include the pore air pressure (u_a). Due to the importance of Terzaghi's principle of effective stress, numerous attempts have been made to extend the theory to unsaturated soils. A compilation of such approaches can be found in Vanapalli (1994).

The most accepted approach to define the stress state of an unsaturated soil was given by Fredlund and Morgenstern in 1977, who showed that any two of three possible stress state variables can be used to define the stress state in an unsaturated soil (Fredlund et al. 1978). The possible combinations are:

1. $(\sigma_n - u_a)$ and $(u_a - u_w)$
2. $(\sigma_n - u_w)$ and $(u_a - u_w)$
3. $(\sigma_n - u_a)$ and $(\sigma_n - u_w)$

Fredlund et al. (1978) suggested that the combination shown below was more appropriate because only one stress variable is affected when the pore-water pressure changes:

$$\begin{bmatrix} (\sigma_x - u_a) & \tau_{yx} & \tau_{zx} \\ \tau_{xy} & (\sigma_y - u_a) & \tau_{zy} \\ \tau_{xz} & \tau_{yz} & (\sigma_z - u_a) \end{bmatrix}$$

and

$$\begin{bmatrix} (u_a - u_w) & 0 & 0 \\ 0 & (u_a - u_w) & 0 \\ 0 & 0 & (u_a - u_w) \end{bmatrix}$$

1.3.1 Soil Suction

Unsaturated soil mechanics combines two independent variables in order to define the state of stress of a soil element. The unsaturated stress state variable that is affected by the amount of moisture within the soil is matric suction, which can be defined as the difference between pore air and pore water pressures, u_a-u_w. The soil suction is then combined with the typical external stress state variable of overburden/structural stress to define the stress state of the soil (Fredlund and Morgenstern 1977). The external stress in unsaturated soil mechanics is referred to as the net normal stress, which is the difference

between the overburden pressure and the air pressure. The air pressure is typically assumed to be atmospheric (i.e., $u_a = 0$) when dealing with soils near the ground surface.

Matric suction, also known as negative pore water pressure, is the pressure that occurs in the voids between soil particles as soil water content decreases. Soil suction is also described as the soil's tendency to retain moisture. In expansive soil, increases in soil suction causes shrinkage in soil total volume. In contrast, as water content increases in the expansive soil, the soil expands. Soil suction is an important parameter in many geotechnical areas such as slope stability, soil expansivity, foundation design, etc. Many laboratory and field methods on how to measure soil suction have been developed. (Nelson and Miller, 1992) Models which incorporate soil suction in the estimation of expansive soil volume change are discussed herein.

1.3.2 Soil Water Characteristic Curves for Unsaturated Soils (SWCC)

The SWCC is the relationship between the change in water content, mass or volume, and the change in soil suction, which represents the energy state. It is used to predict several soil property functions, such as the hydraulic conductivity of an unsaturated soil, shear strength, and modulus of elasticity of the soil. Those predictions are approximate but, in general, satisfactory for unsaturated soil mechanistic problems analysis (Fredlund 2012, Olaiz 2017).

The SWCC can also be used to estimate the equilibrium water content. The most direct way of obtaining the SWCC for a given soil is to measure the suction of a representative sample in the laboratory using filter paper, pressure plate or any other available method. This process may take several days to a couple of weeks depending on the type of soil being tested.

1.3.3 Measuring Soil Suction

There are several ways to measure suction. The most common methods or devices used to measure soil suction are listed in Table 1.1. Included within this table are the types of suction measurable, the range of suction in which the results are reliable, and the weaknesses associated with each device.

Soil suction can be determined either by direct or indirect methods. Direct methods include pressure plates, pressure membranes, suction plates, and tensiometers. These methods measure the pore pressure in the soil or impose a known pressure to the soil and allow the pore pressure to come to equilibrium with the imposed pressure. Indirect methods include filter paper, moisture blocks, thermal conductivity sensors, heat dissipation sensors, and psychrometers. These methods use measurements or indicators of water content or a physical property that is sensitive to a change in water content (e.g., relative humidity, electrical resistance, and rate of heat dissipation). Before suction measurements, a baseline calibration run is made from which all suction measurements are based. Thorough descriptions on methods outlined in Table 1.1 can be referenced Ridley and Wray (1995), and Lee and Wray (1995)

Table 1.1 Methods for Measuring Total and Matric Suction (Ridley and Wray 1995; Fredlund and Rahardjo 1989)

Device	Method (property measured)	Suction measured	Range (kPa)	Main constraints
Thermocouple psychrometer	Indirect (relative humidity)	Total	100 to 7,500	Affected by temperature fluctuations. Sensitivity deteriorates with time.
Thermistor psychrometer	Indirect (relative humidity)	Total	100 to 10,000	Poor sensitivity in the low suction range. Frequent re-calibration is required
Transistor psychrometer	Indirect (Relative humidity)	Total	100 to 71,000	Frequent re-calibration is required. Specimens must be tested in order of increasing suction to avoid hysteresis.
Filter paper (non-contact)	Indirect (Water content)	Total	400 to 30,000	Calibration is sensitive to the elapsed time of the test.
Filter paper (in-contact)	Indirect (Water content)	Matric	Entire range	Automation of the procedure is impossible.
Suction plate	Direct	Matric	0 to 90	Low range of usefulness
Pressure plate	Direct	Matric	0 to 1,500	Range of suction limited by the air-entry value of the plate.
Pressure membrane	Direct	Matric	0 to 1,500	Range in suction is limited by the air-entry value of the membrane.
Standard tensiometer	Direct	Matric	0 to 90	Requires daily maintenance. Temperature fluctuations affect readings. Slow to equilibrate in highly plastic soils.
Osmotic tensiometer	Direct	Matric	0 to 1,500	Reference pressure can deteriorate with time. Temperature dependent.
Imperial College tensiometer	Direct	Matric	0 to 1,800	Range in suction is limited by the air-entry value of the ceramic.
Porous block (Gypsum, nylon, fiberglass)	Indirect (Electrical resistance)	Matric	30 to 3,000	Observations need to be corrected by temperature. Blocks are subject to hysteresis. Response to suction can be slow.
Heat dissipation sensors	Indirect (Thermal conductivity)	Matric	0 to 175	High failure rate. Very fragile
Osmotic cell	Indirect (Osmotic pressure of solutions)	Matric	Not available	Not available

Matric suction can be measured with tensiometers, porous blocks, heat dissipation sensors, suction plates, pressure plates, pressure membranes, and filter paper.

Tensiometers are devices that directly measure the negative pore-water pressure. They are mainly used in the field, although some researchers have used them on instantaneous profile laboratory experiments (i. e., Plagge et al. 1992). Tensiometers consist of a porous ceramic, high air-entry cup connected to a device that measures the pressure (e.g., a mercury manometer, a vacuum gauge, or an electronic pressure transducer). The device is filled with de-aired water. The water in the tensiometer communicates with the soil fluid through the pores in the cup wall. Flow, in or out through the ceramic cup, tends to bring the cup water into hydraulic equilibrium with the soil water (Richards 1965). Unfortunately, standard tensiometers have a limitation in the range they can measure suction, that has been linked, by several authors, to the phenomenon of cavitation in the reservoir water at a tensile stress of about 100 kPa.

Some attempts have been made to extend the range of the tensiometer. Peck and Rabbidge in 1996 used a smaller tensiometer, replaced the water with polyethylene glycol (PEG), and placed a membrane, which is permeable to water but impermeable to the large PEG molecules. This tensiometer has been called osmotic tensiometer. A positive pressure is developed into the reservoir, placing the device in a bath of pure water at atmospheric pressure. Dineen and Burland in 1995 suggested that a small percentage of the PEG molecules could pass through the membrane decreasing the concentration of the solution and lowering the suction (Ridley and Wray 1995).

In 1993, Ridley and Burland pre-pressurized the water in the reservoir, inhibiting the formation of air within the tensiometer. They alleged that little crevices that exist in the tensiometers provide a trap for tiny amounts of air that are released when the tensiometer is placed in a state of tension, forming bubbles in the reservoir. The small size of the tensiometer and the pressurization of the water, run the air trapped into solution. However, the device uses a saturated porous filter that limits the range of suction to its air-entry value of 1,500 kPa (Ridley and Wray 1995).

Pressure plates consist of a pressure chamber, a porous ceramic plate and an air compressor. The soil specimen is placed on a previously saturated porous plate and sealed within the pressure chamber. Under the influence of the applied pressure, the water inside the soil specimen and the ceramic plate will be expelled and collected in a graduated cylinder until equilibrium between the soil specimen and the applied air pressure is reached. At equilibrium, the matric suction of the soil equals the applied pressure (Lee and Wray 1995). The soil suction measurement range of the pressure plate is limited to the air-entry value of the plate.

The pressure membrane apparatus works on the same principle as the pressure plate, except that the soil is placed on a porous membrane rather than a plate. Its range of suction measurements is limited by the air-entry value of the membrane.

Vacuum desiccators consist of a saturated porous ceramic filter disc that separates the soil specimen from a reservoir of water and a mercury manometer. By its suction, the soil will imbibe water from the porous disc, causing a drop in the water pressure in the reservoir, which is measured using the manometer. When

the pore water pressure and the tension in the water of the reservoir are in equilibrium, the flow of water will stop. The range in suction measurements in the suction plate is limited to 100 kPa.

The thermal conductivity sensor is an indirect method of measuring matric suction that consists of a porous ceramic block containing a thermocouple and a miniature heater that delivers a controlled heat pulse. When the water content of the porous ceramic is high, a higher rate of dissipation will be produced and thus a lower temperature rise will be obtained when the mini heater is pulsed. The temperature rise of the sensor can be calibrated against matric suction using a pressure plate apparatus (Lee and Wray 1995).

The thermal conductivity sensor has been used for the in-situ determination of soil suction mainly in North America. Its small range of applicability (0 to 175 kPa) is its main limitation. In addition, a high failure rate has been reported (Oloo and Fredlund 1995).

The porous block works on the principle that the electrical resistance of an absorbent material changes with its moisture content. The block consists of two electrodes buried inside a porous material that is allowed to equilibrate with the soil. Due to a matric gradient between the block and the soil, an exchange of soil water occurs that results in a change in the water content within the sensor, until an equilibrium condition is reached. The electrical resistance of the block is sensitive to the water content of the material. If the electrical resistance is calibrated against known matric suction, the sensor can be used to measure matric suction (Lee and Wray 1995). The calibration is performed by burying the block inside a soil that is subsequently subjected to a known suction inside a pressure plate device (Ridley and Wray 1995).

The materials used as porous materials are gypsum, fiberglass, or nylon, being the gypsum the most suitable medium for the measurement of electrical resistance. Gypsum takes the shortest time to saturate but can suffer from softening when saturated; it is inexpensive, easy to install but a general reduction of electrical resistance has been observed with increasing temperature. Its range is limited to between 50 kPa and 3,000 kPa (Ridley and Wray 1995).

A lesser-known apparatus to determine matric suction is the osmotic cell. Each unit of the osmotic cell consists of a soil chamber separated by a cellophane membrane from chambers that contain a solution with known osmotic pressure. The soil and the solution are allowed to equilibrate. Equilibrium is assumed to occur when no change in the concentration or viscosity of the solution is observed. The specimen is removed, and the water content determined (Livneh et al. 1970).

Finally, the filter paper method uses filter papers as passive sensors to evaluate either total or matric suction. The filter paper is allowed to absorb moisture from a soil specimen. When equilibrium is reached between the soil and the filter paper, the suction in the filter paper will equal the suction in the soil (Ridley and Wray 1995).

If the filter paper is placed in contact with the soil, it will absorb water through capillary flow and the salts in the soil water will travel into the filter paper. For those reasons, the suction measured is matric suction. On the other hand, if the filter paper is placed in a sealed container and it is not allowed to touch the soil, the wetting process will occur by vapor transmission only and the salts will remain in the soil. In this case, the filter paper will measure total suction.

The calibration of the filter paper is achieved by either a) using a pressure plate device, or b) calibrating it against salt solutions of known vapor pressure. A calibration curve for the Fisher Quantitative Coarse Filter Paper is shown in Figure 1.1. The filter paper can determine suctions over the entire range; it is inexpensive and simple. It is also one of the most popular methods to determine suction among practitioners. Its main disadvantage is the extreme difficulty in automating data acquisition, making it a time-consuming method.

The procedure to estimate total suction using filter paper, can be summarized as follows (Nelson and Miller 1992, Amer 2016):
Place a sample of the soil with a calibrated filter paper, where the filter paper should not be in contact with the soil, inside a closed container made of non-corrosive material, such as glass, for at least seven days, so the soil sample and filter paper can equilibrate.
Remove the filter paper and measure the water content by precisely weighing the filter paper before and after oven drying.
Figure 1.1 can be used to determine the total suction value from calculated water content.

The main advantages of this method are that it is inexpensive and can be used over a wide range of suction (up to 150,000 psi or 10^6 kPa). The disadvantage of this method is the degree of accuracy required for weighing the filter paper (0.0001g). The idea is that the humidity inside the container is controlled by soil water content and suction. The filter paper will absorb moisture until equilibrium is reached. Then, the filter paper will have the same suction as that in the soil. This suction value represents the total suction, matric and osmotic suction.

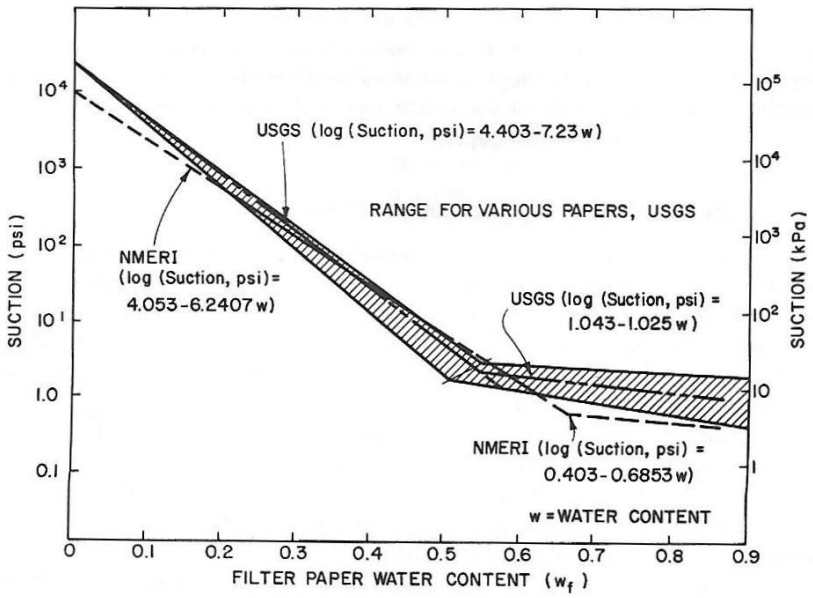

Figure 1.1 Filter paper calibration relationship (After McKeen 1981, Nelson and Miller 1992)

Since the determination of SWCCs involves special testing devices and relatively new procedures, it is

not very widely performed in common engineering practice compared to other well-known tests. Yet, determination of soil suction is a very important task in the field of unsaturated soil mechanics, and therefore, models to predict this property are desirable.

1.3.4 Predicting Soil Suction

Several studies have suggested methods for obtaining the SWCC using grain size distribution (GSD) and other soil properties without direct measurements of the SWCC. Zapata developed a family of SWCCs correlating simple soil properties Figure 1.2, which was initially implemented into the EICM and later revised based on recommendations from the NCHRP 9-23 research project (Zapata et al. 2000, Perera et al. 2005). It is worth noting that this model was developed with a very limited amount of data (about 180 soils). However, more recent research by the PI delivered the results of project NCHRP 9-23A. The primary objective of this study was to collect a database of SWCCs, and other soil properties needed as input in the Pavement ME Design Guide, for the entire continental U.S.A., Hawaii, and Puerto Rico, to aid in the implementation and calibration of the M-E PDG at local conditions. The PI delivered SWCCs for more than 31,000 subgrade materials. This important database, the largest base with unsaturated soil properties ever collected, will be used to assess the moisture content prediction capability of the existing models.

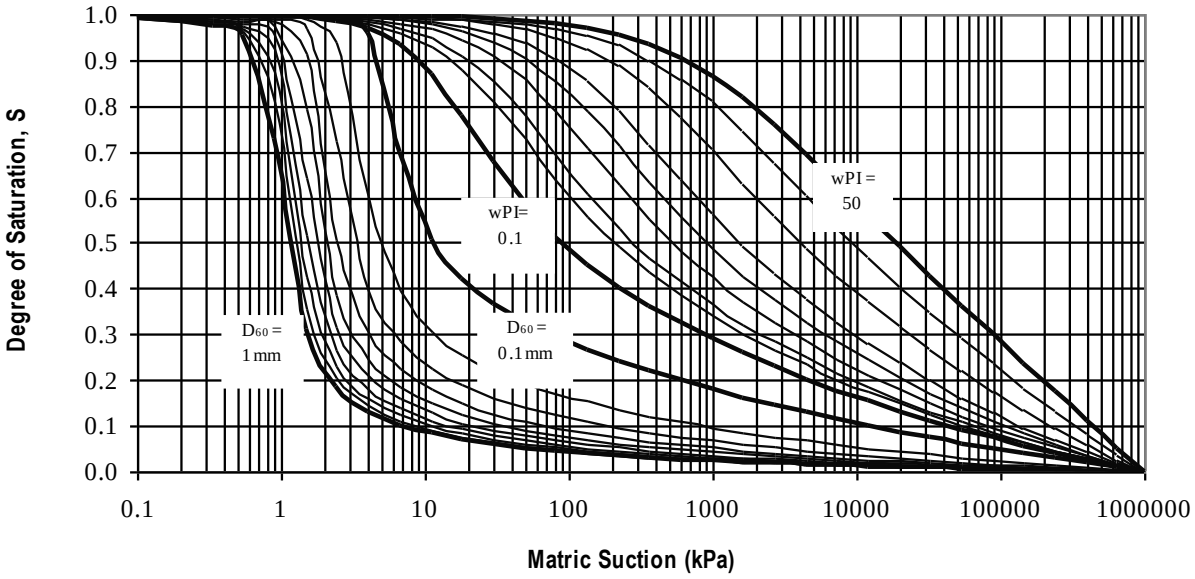

Figure 1.2 Family of Soil-Water Characteristic Curves (after Zapata 2000)

1.3.4.1 Estimating the Equilibrium Suction under Covered Areas

For a relatively near-surface groundwater table, significant potential exists for capillary rise into subgrade soils. The conventional assumption that negative pore water pressures can be estimated by backward extrapolation above the groundwater table of a line of slope equal to the depth times the unit weight of water ($y\gamma_w$) is only appropriate in a thin region above the groundwater table, where soils are wetted to a degree of saturation of 85% or more (Houston et al. 2000). When the groundwater table is relatively deep,

field evidence and numerous numerical modeling studies have shown that even though the pavement structure acts as a cover for the unbound material, its moisture content tends to reach an equilibrium constant value with only minor fluctuations. This constant value is significantly influenced by climate and soil properties. The microclimate above the pavement determines the flux boundary conditions due to lateral flow from shoulders and vertical flow through cracks, especially under high flux rates, and due to evapotranspiration up and across the shoulder (Zapata and Houston 2009).

1.3.4.2 Environmental Boundary Conditions

Environmental conditions have a significant effect on the behavior of both flexible and rigid pavements. External factors such as precipitation, temperature, wind speed, solar radiation, relative humidity, and depth to groundwater table are environment parameters that affect pavement performance. In a pavement structure, moisture and temperature gradients, and freeze/thaw cycles are environmentally driven variables that can significantly affect the pavement layer and subgrade properties and, hence, its stiffness. (Zapata 2018)

Given the complexity and large number of climatic parameters affecting the flux boundary conditions, it was necessary to represent its effect in a relatively simpler way. In 1948, Thornthwaite introduced the Thornthwaite Moisture Index (TMI) as an index that classified the climate of a given location (McKeen and Johnson 1990). The TMI quantifies the aridity or humidity of a soil-climate system by summing the effects of annual precipitation, evapotranspiration, storage, deficit, and runoff. To a significant degree, the TMI index balances lateral infiltration and evapotranspiration for a particular region. TMI can be found from Figure 1.3, which presents a contour map with TMI values (Lytton et al. 1990):

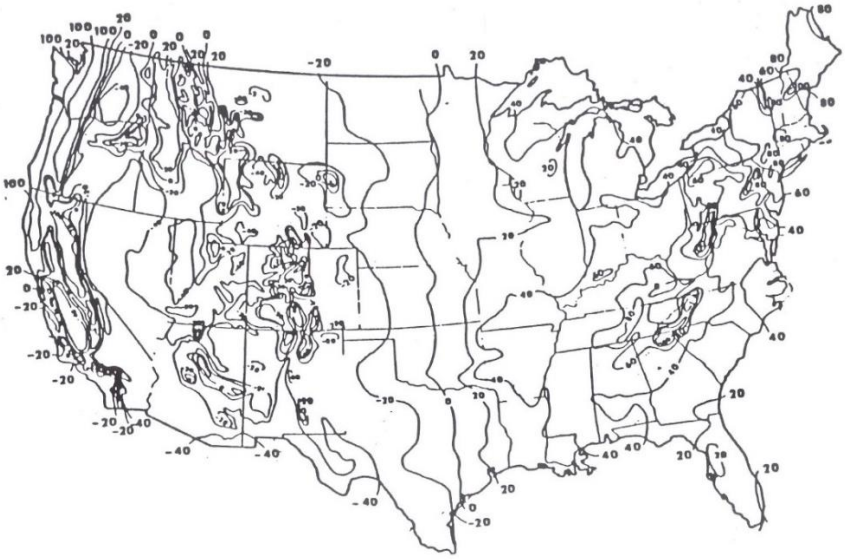

Figure 1.3 Thornthwaite Moisture Index contour map

The parameter that has been accepted by geotechnical engineering for quantifying the climatic conditions is the Thornthwaite Moisture Index, or TMI (Thornthwaite, 1948).

1.3.4.3 Thornthwaite Moisture Index, TMI

Thornthwaite Moisture Index, TMI, is a parameter found based on climatic data, usually collected from

weather stations. It is used to evaluate the soil moisture of the unsaturated layer. The importance of TMI is its ***relation*** to water suction. (Yue et al. 2014) In other words, the depth of design soil suction changes can be predicted based on the TMI value (Sun et al. 2017). The original equation of TMI proposed by Thornthwaite in 1948 is written as follows:

$$TMI = \left(\frac{100SP - 60D}{PET}\right)$$

According to the equation, TMI is affected by water surplus, SP, water deficiency, D, and potential evapotranspiration, PET, or the water need. Since they occur in different seasons, SP and D affect the TMI in such a way that one is positive and the other is negative (Thornthwaite 1948). The deficiency is 60% of the surplus and the reason, as explained by Thornthwaite, is "Water surplus means seasonal additions to subsoil moisture and ground water. Deeply rooted perennials may make partial use of subsoil moisture and thus minimize the effect of drought. Transpiration proceeds, but at reduced rates. For this reason, a surplus of only 6 inches in one season and counteract a deficiency of 10 inches in another. Thus, in an over-all moisture index the humidity index has more weight than the aridity index: the latter has only six-tenths the value of the former" (Thornthwaite 1948).

Evapotranspiration is a combination of evaporation and transpiration from plants, which is the opposite of precipitation where the water is moved from earth back to the atmosphere. The potential evapotranspiration is explained by Thornthwaite as follows: "The vegetation of the desert is sparse and uses little water because water is deficient. If more water were available, the vegetation would be less sparse and would use more water. There is a distinction, then, between the amount of water that transpires and evaporates and that which would transpire and evaporate if it were available. When water supply increases, as in a desert irrigation project, evapotranspiration rises to a maximum that depends only on the climate. This we may call "potential evapotranspiration," as distinct from actual evapotranspiration" (Thornthwaite 1948).

According to Sun, PET "...was developed based upon global climate pattern distribution and the concept of plant physiology relating to moisture availability." (Sun et al. 2017) As proposed by Thornthwaite, PET can be calculated using the following equation (Zareie et al. 2016):

$$PET\ (cm) = f_1 \times f_2 \times 1.6 \times \left(\frac{10\ t}{I}\right)^a$$

where,
f_1 is the fraction of the number of days in month divided by the average number of days in month, 30; f_2 is the fraction of the number of hours in a day divided by the base of 12 h in a day; t is the mean monthly temperature in degrees Celsius; I is the annual heat index; and a is a coefficient.

$$I = \sum_{i=1}^{12} \left(\frac{t_i}{5}\right)^{1.514}$$

where,

t_i is the mean temperature for the i^{th} month

$$a = (6.75 \times 10^{-7})\, I^3 - (7.71 \times 10^{-5}) I^2 + (1.792 \times 10^{-2}) I + 0.49239$$

In 1955, Thornthwaite and Mahther modified the TMI equation to be:

$$TMI = 100\left(\frac{P}{PET} - 1\right)$$

where,
P is the annual precipitation.

In 2006, Witczak et al. modified the TMI equation to be (Witczak et al. 2006):

$$TMI = 75\left(\frac{P}{PET} - 1\right) + 10$$

When the precipitation is greater than the evaporation, the TMI is positive, while negative TMI values represent arid and semi-arid regimes. As defined by Thornthwaite, the TMI represents an average annual condition; while the modified TMI equation can be used to represent daily, monthly, or annual conditions for any given location (Zapata 1918).

Karunarathne (2016) conducted a sensitivity study on the effects of the number of years of data, or averaging period, used in the calculation of the TMI. Figure 1.4 from the study illustrates how the variability in TMI significantly increases from a 25-year duration to a yearly duration.

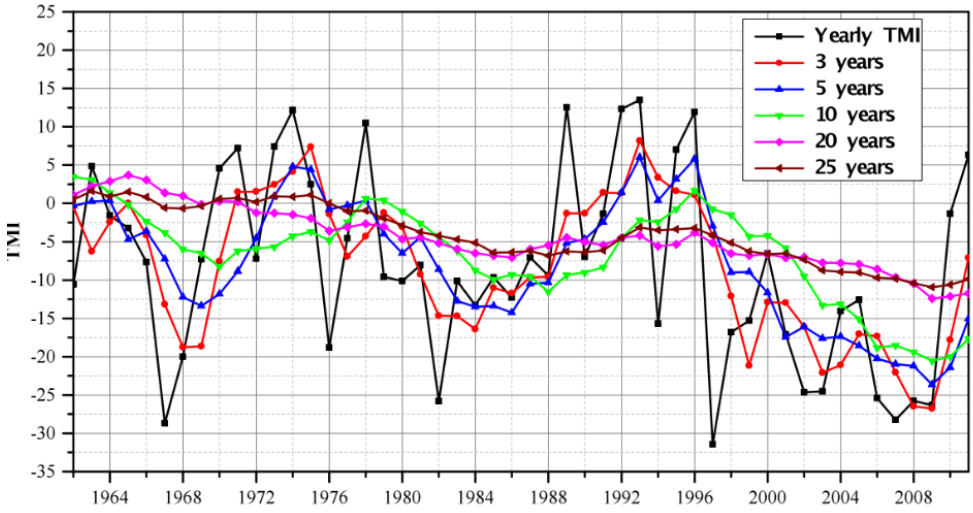

Figure 1.4 Sensitivity of averaging period on TMI (Karunarathne 2016)

1.3.4.4 Predicting Equilibrium Matric Suction under Pavement Structures

Researchers have shown that the moisture content beneath pavements reaches an equilibrium condition several years after construction (Aitchison and Richards 1965, Basma and Ai-Suleiman 1991, Richards

1965). In order to model water movement in the unbound materials, it is necessary to link the initial and flux boundary conditions imposed by climatic changes to the internal stress state of the material. Almost all covered areas encountered in engineering practice are built near the surface covering unsaturated soil masses that would most probably stay unsaturated during the lifetime of the structure. Suction significantly affects the total head for flow and the hydraulic conductivity in unsaturated soils by directly controlling their moisture retention capabilities. Therefore, to consider the effect of moisture changes on shear strength and resilient modulus, the soil's matric suction must be characterized. The suction beneath covered areas is mainly dependent on climatic factors and soil index properties (Russam and Coleman 1961, Coleman 1965, Fredlund and Rahardjo 1993, Zapata 1999).

1.3.4.5 Post-Tensioning Institute 3rd Edition

The Post-Tensioning Institute 3rd Edition (2004, 2008), published, with the aid of Dr. Lytton, a relationship of equilibrium suction and TMI, from the accumulation of several previous studies including Bryant (1998), Wray 1989), and McKeen (1981). The relationship is shown in Figure 1.5.

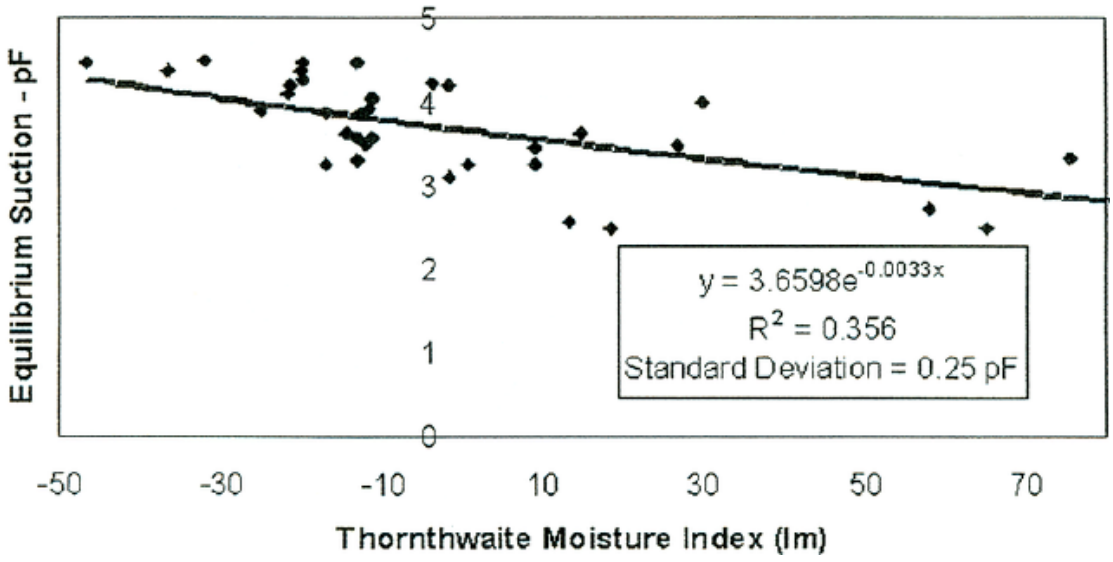

Figure 1.5 Equilibrium Suction vs. TMI (Post-Tensioning Institute 3rd Edition 2008)

1.3.4.6 Perera (2003) Model

As part of the NCHRP 9-23 project entitled *Environmental Effects in Pavement Mix and Structural Design*, material samples were collected from beneath the highway pavement of two WesTrack cells, one MnRoad section, and 27 Long-Term Pavement Performance (LTPP) sites located throughout the United States (LTPP 2003, Houston et al. 2006). The sites were selected to represent an unbiased statistical distribution with respect to factors such as pavement type, depth to groundwater table, mean annual temperature, precipitation, freezing conditions, soil type, and presence of cracking (Perera 2003, Perera et al. 2004a).

In 2003, Perera made a study that relates in-situ moisture content, suction, TMI, and index soil properties. He developed correlations for two models: the *TMI-*P_{200} model, which is valid for granular base materials; and the *TMI-*P_{200}*/wPI* model, used to estimate the equilibrium suction of subbase and subgrade materials

(Rosenbalm 2011). The two models are briefly explained in the following paragraphs.

1.3.4.7 TMI-P200 Model

This model is used to find the equilibrium soil suction based on every aspect that affects water content, such as climate conditions (represented by TMI) and percent passing the #200 sieve. The following equation was presented:

$$\Psi = \alpha + e^{[\beta+\gamma(TMI+101)]}$$

where,
Ψ – the matric suction of the soil; and α, β, γ are regression constants.

The values of P_{200} range between zero and sixteen percent. If more than 16% passes sieve #200, P_{200} is limited to16%. The regression constants can be found in Table 1.2 and interpolation between values is allowed (Perera 2003).

Table 1.2 TMI-P200 Regression Constants (Perera 2003)

P_{200}	α	β	γ
0	3.649	3.338	-0.05046
2	4.196	2.741	-0.03824
4	5.285	3.473	-0.04004
6	6.877	4.402	-0.03726
8	8.621	5.379	-0.03836
10	12.180	6.646	-0.04688
12	15.590	7.599	-0.04904
14	20.202	8.154	-0.05164
16	23.564	8.283	-0.05218

For programming purposes, Rosenbalm developed the following equations to estimate the regression constants (Rosenbalm 2011):

$$\alpha = -0.00157(P_{200})^3 + 0.110566(P_{200})^2 - 0.11352(P_{200}) + 3.8218$$

$$\beta = -0.0044713(P_{200})^3 + 0.112094(P_{200})^2 - 0.33636(P_{200}) + 3.2358$$

$$\gamma = 2.87563 \times 10^{-5}(P_{200})^3 - 0.00085(P_{200})^2 + 0.006108(P_{200}) - 0.04977$$

1.3.4.8 TMI-P_{200}/*w*PI model

This model was developed for fine grained material, which makes it suitable for expansive soils. For such

materials, in addition to P_{200}, the weighted plasticity index, *w*PI, property was added, where:

$$wPI = \frac{PI \times P_{200}\%}{100}$$

The following equation is used to calculate suction based TMI, P_{200}, and *w*PI (Perera 2003).

$$\Psi = e^{\left[\frac{\beta}{TMI+\gamma}\right]} + \delta$$

where,

Ψ is the matric suction of the soil; and $\alpha, \beta, \gamma, and\ \delta$ are regression constants.

Table 1.3 presents the values of the regression constants for this model. In cases where the *wPI* value is less than 0.5 and P_{200} is less than 10, the *TMI-P_{200}* model should be used. The regression constants shown in Table 2 were developed as part of the NCHRP 9-23 project, which updated the original parameters that Perera presented in 2003 (Rosenbalm 2011).

Table 1.3 TMI-P200/WPI Regression Coefficients

P_{200}	*w*PI	$\boldsymbol{\alpha}$	$\boldsymbol{\beta}$	$\boldsymbol{\gamma}$	$\boldsymbol{\delta}$
10		0.3	419.07	133.45	15.0
50	0.5	0.3	521.50	137.30	16.0
	5.0	0.3	663.50	142.50	17.5
	10	0.3	801.00	147.60	25.0
	20	0.3	975.00	152.50	32.0
	50	0.3	1171.2	157.50	27.8

Rosenbalm developed equations for each regression constant. These equations are used when *w*PI is less than 0.5 (Rosenbalm 2011):

$$\beta = 2.56075(P_{200}) + 393.4625$$

$$\gamma = 0.09625(P_{200}) + 132.4875$$

$$\delta = 0.025(P_{200}) + 14.75$$

The following equations are used when *w*PI ≥ 0.5:

$$\beta = 0.006236(wPI)^3 - 0.7798334(wPI)^2 + 36.786486(wPI) + 501.9512$$

$$\gamma = 0.00395(wPI)^3 - 0.04042(wPI)^2 + 1.454066(wPI) + 136.4775$$

$$\delta = -0.01988(wPI)^2 + 1.27358(wPI) + 13.91244$$

It is to be noted that in his dissertation, Perera mentioned that only the drying branch of the SWCC curves were used in his study. He wrote in the Future-Research-section: "The wetting curve of the soil should be evaluated to identify the magnitude of hysteresis associated with different soil types and thereby assess the validity of the assumption that the hysteresis is insignificant." (Perera 2003) In addition, Fredlund in his book, Unsaturated Soil Mechanics in Engineering Practice, wrote "The water content versus matric suction curves for any porous material are not the same during wetting and drying" (Fredlund 2012). According to Fredlund (1999), Feng used GCTS-type thermal conductivity suction sensors to study the difference between the drying and wetting calibration curves due to hysteresis. He came up with the following mathematical equation (Fredlund 2012):

$$\Delta\psi^* = \frac{\psi_d - \psi_w}{\psi_w} \times 100$$

where,
$\Delta\psi^*$ is the percent change in suction between drying and wetting calibration curves; ψ_d is the suction on the main drying calibration curve; and ψ_w is the suction on the main wetting calibration curve.

In addition, Feng found an approximate relation between drying and wetting suctions based on experimental test results as shown in Figure 1.6 and summarized it with the following equation (Fredlund 2012):

$$\psi_w = 0.70\,\psi_d$$

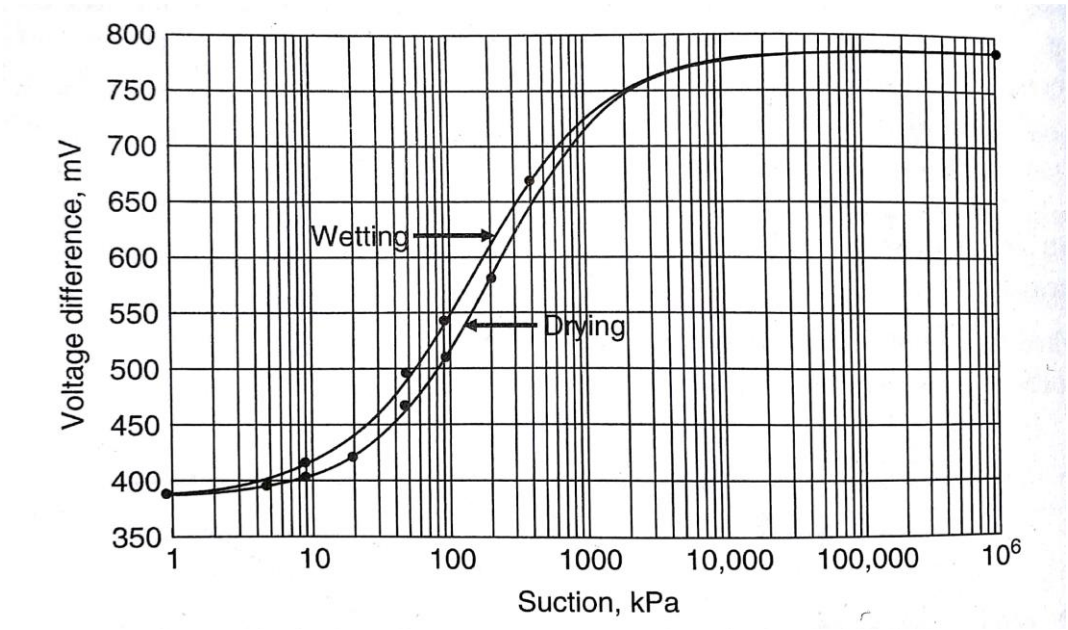

Figure 1.6 Typical hysteresis measured on FTC-100 thermal conductivity soil suction sensors (Fredlund 2012, after Feng et al. 2002)

1.3.4.9 Vann (2019) Model

Vann 2019 improved the work of Lytton and the PTI, with the addition of several new equilibrium moisture content measurements from the Cuzme 2018 study. Data is shown in Figure 1.7 below.

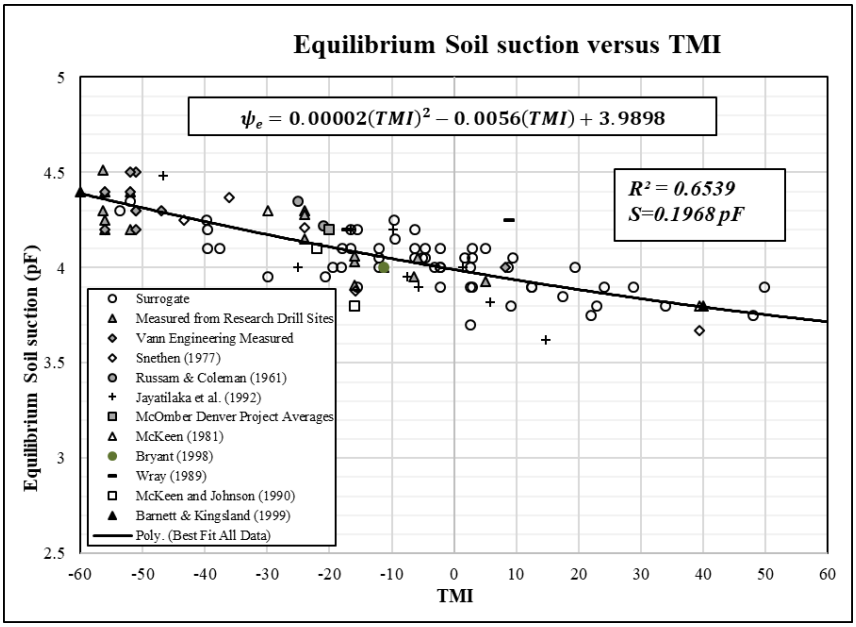

Figure 1.7 Equilibrium Suction vs. TMI with Literature Suction Values (Vann 2019)

1.3.4.10 Summary of Soil Volume Change Prediction Methods

The determination of the magnitude of potential soil volume change is a key focus of geotechnical engineering as it causes significant infrastructure damage each year. Studies have been published, which empirically relate soil index properties (Atterberg limits, gradation, mineralogy, etc.), along with soil engineering properties (density, moisture content, swell pressure, etc.), to volume change. Such studies, which have been reviewed by the authors, include: Seed et al. (1962), van der Merve (1964), Ranganatham and Satyanarayana (1965), Komornik and David (1969), Nayak and Christensen (1971), Vijayvergiya and Ghazzaly (1973), Schneider and Poor (1974), McCormack & Wilding (1975), Brackely (1975b), O'Neil & Ghazzally (1977), Chen (1975), Johnson (1978) Weston (1980), Bandyopadhyay (1981), Picornell and Lytton (1984), Dhowian (1990a), Basma (1993), Cokca (2002), Erguler and Ulusay (2003), Rao et al. (2004), Erzin and Erol (2004), Sabtan (2005), Azam (2007), Yilmaz (2009), Turkoz & Tosum (2011), Cimen et al. (2012), Zumrawi (2013).

Direct laboratory measurements of the volume change potential of a soil help improve the estimation of potential volume change in the field. The 1-D oedometer "Response to Wetting Test" as described in ASTM D4546 is the common type of laboratory test for volume change determination. One key difference from the laboratory oedometer test compared to the field conditions the soil will experience is the final degree of saturation. The response to wetting test inundates the sample, driving to almost full saturation. However, the probability that the soil will reach this moisture level over the period of the structure/pavements design life is very low (Houston and Houston 2017). The following studies, which include 1-D oedometer test-base relationships, have been reviewed by the authors as part of this study: Jennings and Knight (1957), De Bruijn (1961, 1965), Burland (1962) Sampson et al. (1965), Noble (1966), Sullivan and McCelland (1969), Komornik et al. (1969), Holtz (1970), NAVFAC (1971), Wong & Yong (1973), Gibbs (1973) Jennings et al. (1973), Smith (1973), Teng et al. (1972, 1973), Teng & Clisby (1975), Porter & Nelson (1980), Fredlund et al. (1980), Sridharan et al. (1986), Erol et al. (1987), Shanker et al. (1987), Nelson et al. (1998, 2001), Al-Shamrani & Al-Mhaidib (1999), Basma et al. (2000), Subba Rao & Tripathy (2003)

One of the widely used methods for volume change estimation is the Potential Vertical Rise published by the Texas Department of Transportation (TxDOT-12-E, 1978), which includes both empirical-based relationships and results from an oedometer test. In 2005, the Texas DOT updated the approach to determining the volume change of expansive soils using the work of Lytton, Aubeny and Bulut (2005), which encompassed a suction-based approach. The study concluded that the previous empirical-based approach significantly overestimated the soil heave and did not account for the shrinkage of the soil during dry climatic periods. Numerous other researchers have published studies on suction-based approaches to determine the volume change of expansive soils including but not limited to: Aitchison (1983), Johnson and Snethan (1978), Snethan (1980), Mitchell & Avalle (1984), Hamberg & Nelson (1984), Dhowian (1990), Fityus & Smith (1998), Briaud et al. (2003), Lu (2010), Tu & Vanapalli (2015, 2016).

The suction-based approach by Lytton, Aubeny, and Bulut (2005) for estimating the volume change of expansive soils which was adopted by the Texas DOT and the Post-Tensioning Institute for the design of slabs on ground (PTI, 2004, 2008), was the accumulation of efforts of several related studies including: Lytton (1977), McKeen & Hamberg (1981), Holtz & Kovacs (1981), Cover & Lytton (2001), Lytton et al.

(2004). The approach encompasses the volumetric strain caused by changes in both stress states of the soil (matric suction and net normal stress). The relationship between the change in each stress state and the volumetric strain, referred to as the compression indices, must be directly measured or empirically determined.

The second approach to estimating expansive soil volume change will involve the work of Singhal (2011), and Houston and Houston (2017), which use a suction-oedometer-based approach. The method, referred to as the Surrogate Path Method by Singhal (2011), uses a response to wetting test (ASTM D4546) with an estimated suction envelope to estimate the volume change of the soil. The intriguing aspect of the Surrogate Path Method is that neither compression index needs to be measured or estimated. Olaiz (2017) and Vann et al. (2018) conclude that the Surrogate Path Method compares statistically well with the true measured volumetric strain of expansive soil.

The Lytton, Aubeny and Bulut (2005) approach and the Surrogate Path Method (Singhal, 2011), will be summarized in further detail herein, as they are the two methods of estimating soil volume change that the authors will explore and incorporate in this study. Each method requires that the suction envelope, or active zone, of the soil profile be known.

1.4 Active Zone (Depth of Influence)

The key aspects which affect the volume change potential of soil are the climatic conditions of the site and the soil properties. The two aspects directly affect the active zone, or depth of influence, of the soil profile, illustrated in the figure below.

The change in water content occurs in the unsaturated zone of the subsurface. However, at some depth, no dramatical change in water content occurs. In other words, the change in suction decreases with depth until reaching a point where it is almost zero, or the water content becomes nearly constant and does not change with depth (Figures 1.8 and 1.9) (Nelson and Miller 1992 and Bulut 2001). The depth to the zero-suction-change is known as the depth of influence or the active zone. Other definitions can be found in the literature for the active zone such as the zone of seasonal moisture fluctuation, the depth of wetting, or the depth to constant/equilibrium suction.

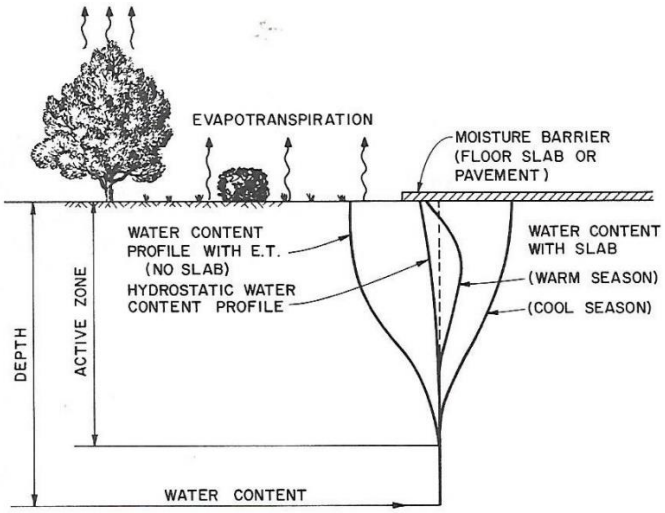

Figure 1.8 Water content profile in the active zone (After Nelson and Miller 1992)

Other factors that influence the depth of the active zone are the site cover (i.e., structure, pavement, vegetation, etc., groundwater table and soil cracking pattern, and the amount of clay minerals within the soil profile.

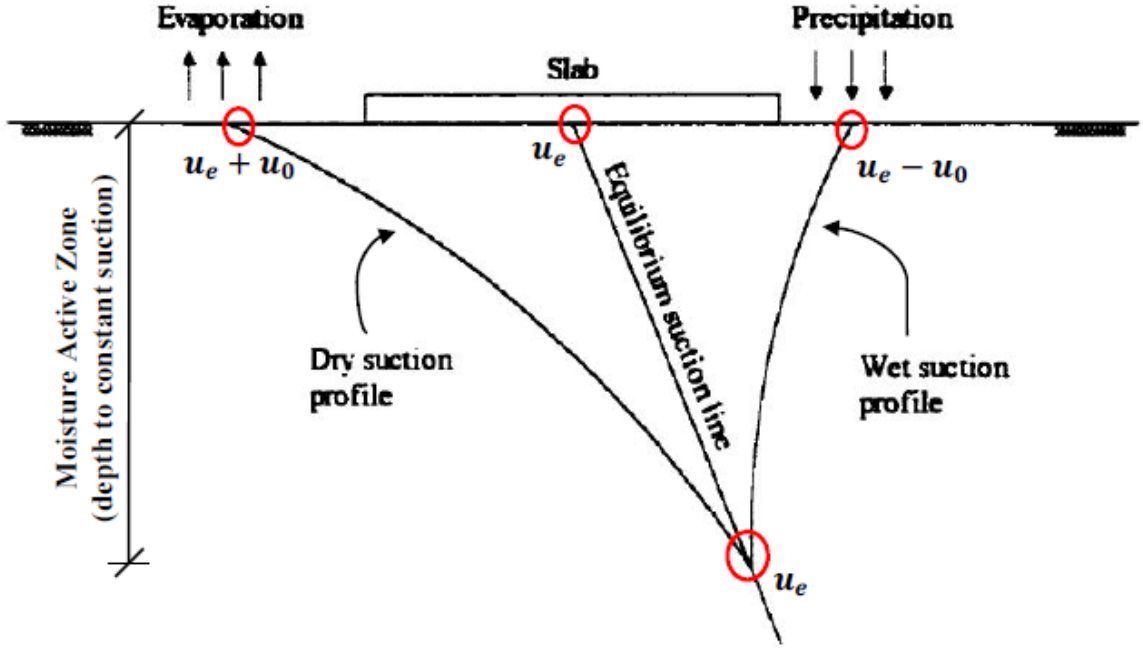

Figure 1.9 Suction profiles, modified from Bulut 2001 (After Amer 2016)

Based on those factors, it can be realized that the active zone is not constant. Underestimating the depth of the active zone may cause an underestimation of the potential volume change. Therefore, many studies have been found in the literature that try to define the active zone. There are four main components to the active zone or suction envelope:

1. The change of suction at the surface, referred to as the **surface flux**, is directly affected by the climatic conditions and can be altered due to site cover.
2. The depth which corresponds to a negligible change in soil suction, referred to as the **depth to equilibrium suction.**
3. The magnitude of equilibrium suction
4. The maximum and minimum suction values at any given depth within the suction profile, referred to as the **shape of the suction envelope.**

Extensive research has been completed on suction envelopes including: Mitchell (1980, 2008, 2013), McKeen and Johnson (1990), Fityus et al. (1998, 2004), Barnett and Kingsland (1999), Fox (2000) Cameron (2001), Jaksa et al. (2002), Briaud et al. (2003), McManus et al. (2004), Aubeny and Long (2007), Chan and Mostyn (2008), Vanapalli and Lu (2012), Karunarathne et al. (2012), Li et al. (2013), Sun (2017), and Lopes and Karunarathne (2017), and the Post-Tensioning Institute 2nd and 3rd Edition (1996, 2004, 2008). Additional methods, which the authors of this study will incorporate in the approach for volume change estimation, are summarized in more detail herein.

1.4.1 Surface Flux

The first component to produce the suction envelope, or active zone shown previously in Figure 1,9, is the magnitude of the suction change at the surface, also called the surface flux. The Australian Standard for Residential Slabs and Footings, or AS2870 (1996, 2011), have proposed methods for determining the surface flux for a given site. Figure 1.10 summarizes the work that was used to determine the surface flux values based on TMI for the 2001 update to AS2870.

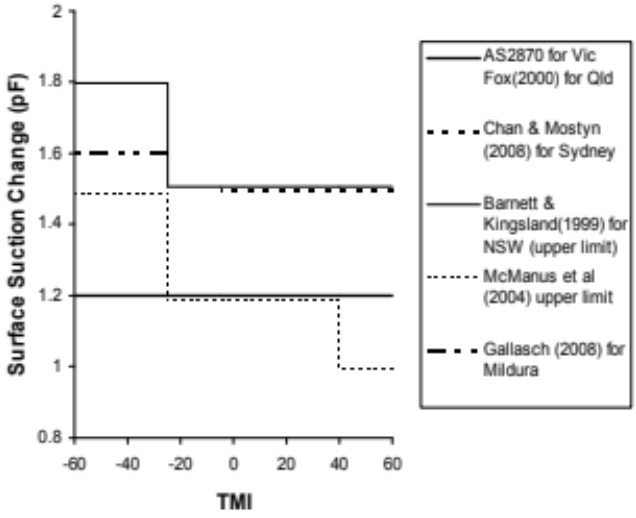

Figure 1.10 Relationship between the Design Surface Soil Suction Change (Δu) and TMI (Mitchell 2008)

Vann 2019 improved the relationship between the soil suction change at the surface and TMI using the previous work of the Mitchell, the Australian Standard, and additional data of long-term moisture/suction monitoring from Cuzme 2018. The relationship is shown in Figure 1.11 below.

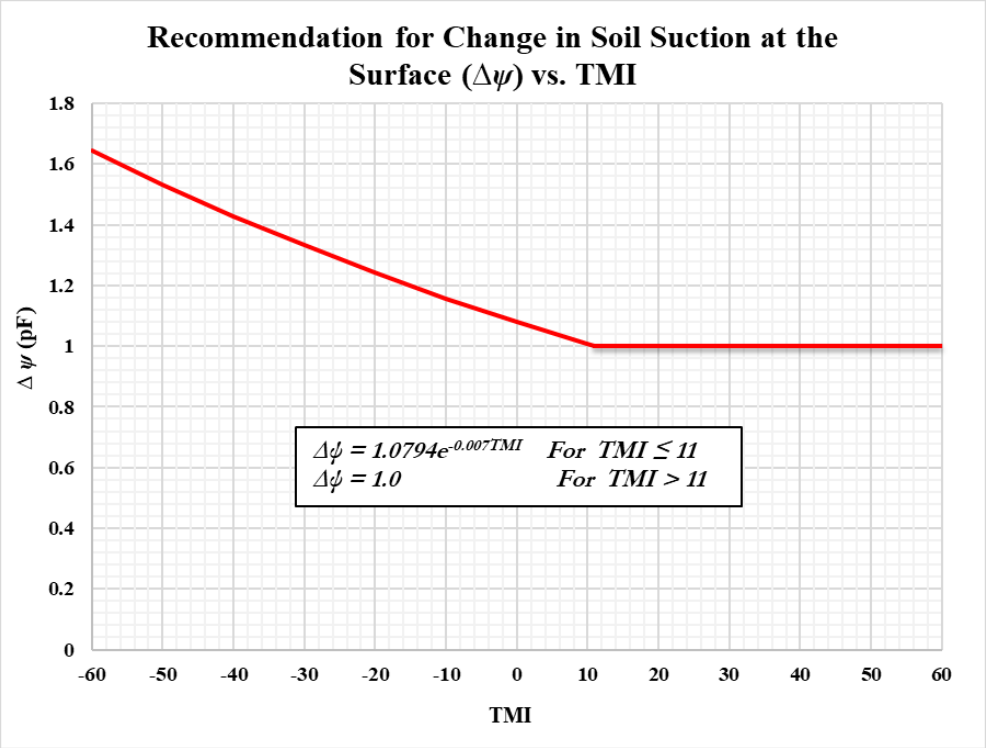

Figure 1.11 Relationship between the Design Surface Soil Suction Change (Δu) and TMI (Vann 2019)

The authors of this study have proposed a new method for determining the surface flux, which will incorporate a statistical study of how the Thornthwaite Moisture Index changes with time and will estimate the possible suction values at the surface using the previously described Perera (2003) empirical correlation.

1.4.2 Depth to Equilibrium Suction

Vann 2019 also improve the relation between the depth of equilibrium suction and TMI (Figure 1.12). The relationship using the data from Cuzme 2018 and previous studies which have been included in the development of the Post-Tensioning Design of Slabs on Ground (2006) and AS2780 (2011).

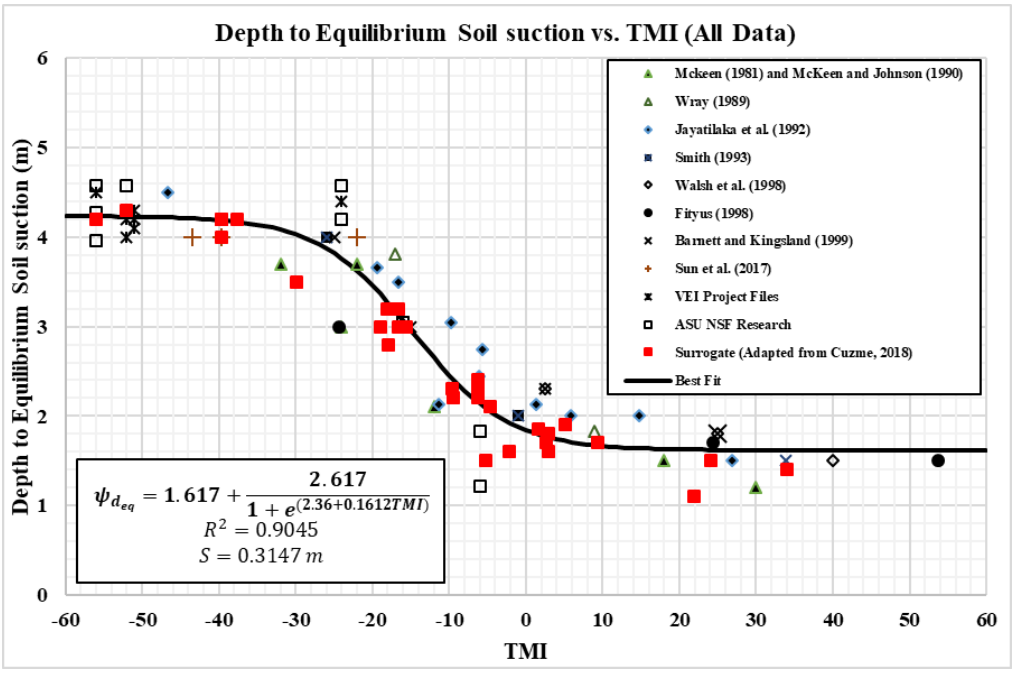

Figure 1.12 Relationship between the depth Equilibrium Soil Suction and TMI (Vann 2019)

Vann et al. (2018) conducted a study, which sought to improve the above relationship between the depth equilibrium suction and TMI. He utilizes water content and routinely measured soil index properties, such as the liquid limit (LL) to estimate suction profiles in the field. The suction estimate (Figure 1.13) can be used to verify the estimated depth of equilibrium suction or to determine the in-situ suction profile.

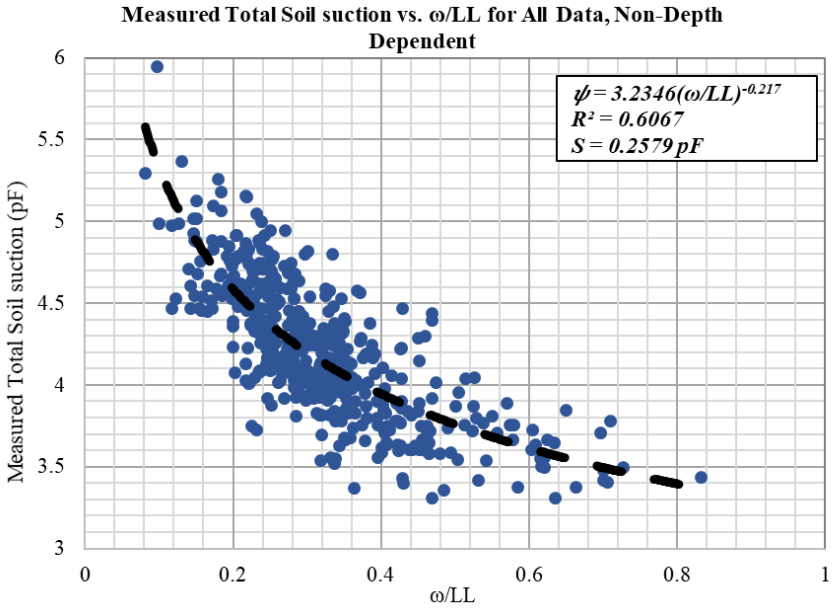

Figure 1.13 Soil Suction Estimation (Vann et al. 2018)

1.4.3 Shape of the Suction Envelope

The final attribute to producing the suction envelope is determining the change in suction as at a given depth in the soil profile. Mitchell (1979) developed a one-dimensional solution for periodic surface soil suction, which varies in a sinusoidal manner in response to climate cycles (as a function of time). The Mitchell (1979) equation is:

$$u(y,t) = U_e - U_o exp\left\{-\left[\left(\frac{n\pi}{\alpha}\right)^{0.5}\right]y\right\} cos\left\{2n\pi t - \left[\left(\frac{n\pi}{\alpha}\right)^{0.5}\right]y\right\}$$

where,

$u(y,t)$ is the suction as a function of space, *y*, and time, *t*, in pF or kPa; U_e is the equilibrium suction below the active zone depth, in pF or kPa; U_o is the amplitude of the soil suction variation, in pF or kPa; *n* is the frequency number; α is the diffusion coefficient in cm^2/sec; *t* is the time coordinate in days; and *y* is the space coordinate for depth in meters of feet

The Mitchell (1979) method produces a suction profile, which is symmetric about the magnitude of constant suction value. Aubeny and Long (2007) improved the method to allow the profile to be skewed based on the climatic conditions of the site (Figure 1.14). Theoretical examples of how the skewness of humid, semi-arid, and arid climates differ are depicted in the figure below.

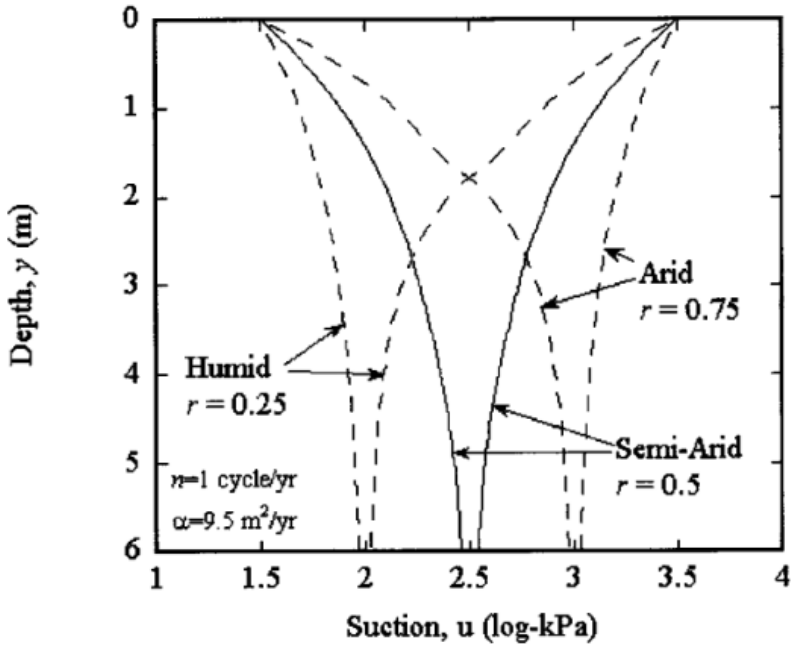

Figure 1.14 Characteristic suction envelopes for humid, semi-arid, and arid climates (Aubeny and Long 2007)

One key soil parameter necessary for the suction envelope computation summarized above is the soil diffusion coefficient. In 2008, Mitchell performed a study, which resulted in the following relationship between TMI and the diffusion coefficient, shown below.

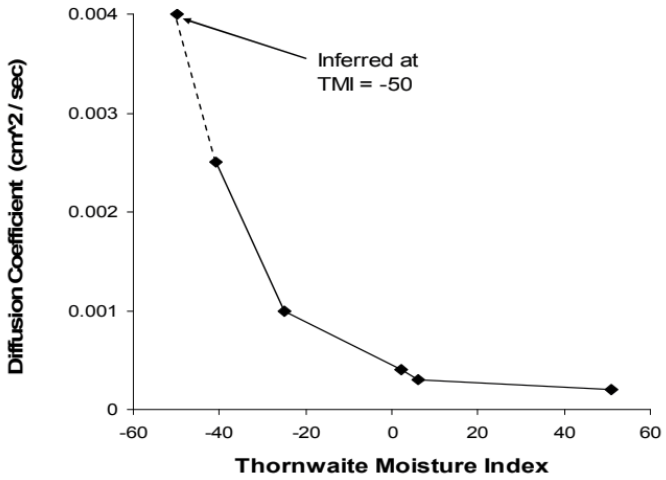

Figure 1.15 Relationship between Diffusion Coefficient and TMI (Mitchell 2008)

The diffusion coefficient can also be back calculated for a given site if the surface flux, magnitude of equilibrium suction, depth to equilibrium suction and the variation of soil suction at the depth of equilibrium suction (Lytton 2004 recommends 0.2 pF).

Alterations to the suction profile have also been studied and proposed. Alterations include post-construction drainage changes such as a sloping grade, replacing the native expansive soil with imported granular soil, vegetation, and natural desiccation cracking. Lytton, Aubeny and Bulut (2005) developed changes to the Mitchell (1979) suction envelope method to encompass such scenarios. Figures 1.16 and 1.17 present two example profiles from Lytton, Aubeny and Bulut (2005), which the natural suction profile is altered due to the addition of granular soil and the presence of deep roots from adjacent vegetation.

Efforts to simplify the development of the suction envelope have been a focus of the associated research in the past two decades. A triangular envelope, which linearly interpolates from the surface flux to the depth of equilibrium suction has been incorporated into AS2870 (2011). Figure 1.18 depicts the simplified suction envelope from AS2870, as well as their published alterations to the profile based on the proximity of nearby trees.

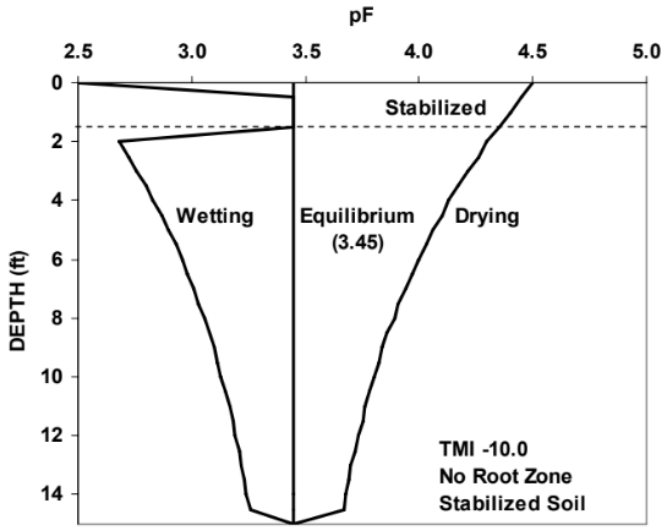

Figure 1.16 Suction Profile versus Depth with Adding Stabilized Layer, Fort Worth North (Lytton, Aubeny and Bulut 2005)

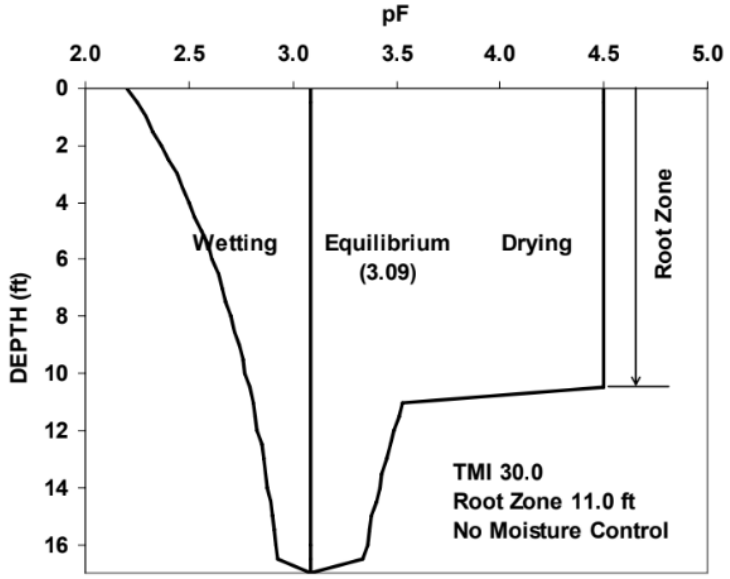

Figure 1. 17 Suction Profile versus Depth for the Case of No Moisture Control, Atlanta US 271 (Lytton et al. 2005)

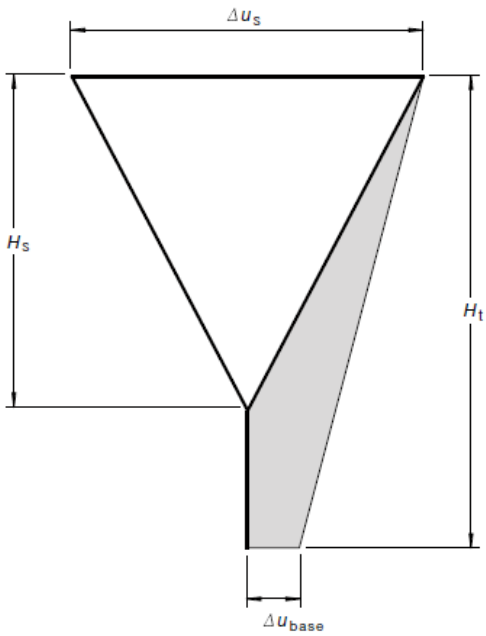

Depth of design suction change, (H_s)	Single tree		Tree group	
	Maximum extra suction change (Δu_{base})	Maximum design drying depth (H_t)	Maximum extra suction change (Δu_{base})	Maximum design drying depth (H_t)
m	pF	m	pF	m
1.5	0.30	2.5	0.38	3.0
1.8	0.33	2.7	0.40	3.3
2.3	0.35	3.0	0.43	3.6
3	0.38	3.4	0.46	4.1
4	0.43	4.0	0.55	4.5

Figure 1.18 Design Soil Suction Change Distribution with Depth for Tree Drying Effects for Different Climate Zones (AS2970-2011)

The depth and time dependent suction envelope equation originally developed by Mitchell (1979) and improved by Aubeny and Long (2007), will be used in this study to help build the suction profile. The profiles will be compared to those produced in the simplified method proposed by the Australians (AS2870, 2011).

1.4.4 Key Components of Lytton, Aubeny and Bulut (2005) Strain Model

The most widely accepted method for estimating volumetric strain is the one developed for the Texas DOT and the Federal Highway Administration, FHWA, by Lytton et al. in 2005, which is as follows:

$$\frac{\Delta V}{V} = -\gamma_h log_{10}\left(\frac{h_f}{h_i}\right) - \gamma_\sigma log_{10}\left(\frac{\sigma_f}{\sigma_i}\right) - \gamma_\pi log_{10}\left(\frac{\pi_f}{\pi_i}\right)$$

where,

$\frac{\Delta V}{V}$ is the volumetric strain (volume change with respect to initial volume); γ_h is the the matric suction compression index; γ_σ is the mean principal stress compression index; γ_π is the osmotic suction

compression index; h_i is the initial matric suction; h_f is the final matric suction; $\sigma_i$is the initial mean principal stress; σ_f is the final mean principal stress; π_i is the initial osmotic suction; and π_f is the final osmotic suction.

Although, total suction is the sum of matric suction and osmotic suction, Fredlund wrote "Matric suctions in a soil mass change is a result of moisture infiltration and evaporation at the ground surface. Osmotic suction in the soil does not appear to be highly sensitive to modest changes in the water content of the soil. As a result, a change in the total suction is quite representative of a change in the matric suction." (Fredlund 2012). Also, Lytton wrote: "It is the change of matric suction that generates the heave and shrinkage, while osmotic suction rarely changes appreciably." (Lytton 2005) Thus, the change in matric suction is responsible to shrinkage and heave and osmotic suction does not affect enough to be concerned. (Lytton 2005, Fredlund 2012) Thus, the equation can be rewritten as:

$$\frac{\Delta V}{V} = -\gamma_h log_{10}\left(\frac{h_f}{h_i}\right) - \gamma_\sigma log_{10}\left(\frac{\sigma_f}{\sigma_i}\right)$$

1.4.4.1 Suction Compression Index, γ_h

The Suction compression index, γ_h, is a parameter used to relate total suction to volume change to predict heave or shrinkage in expansive soils as illustrated below:

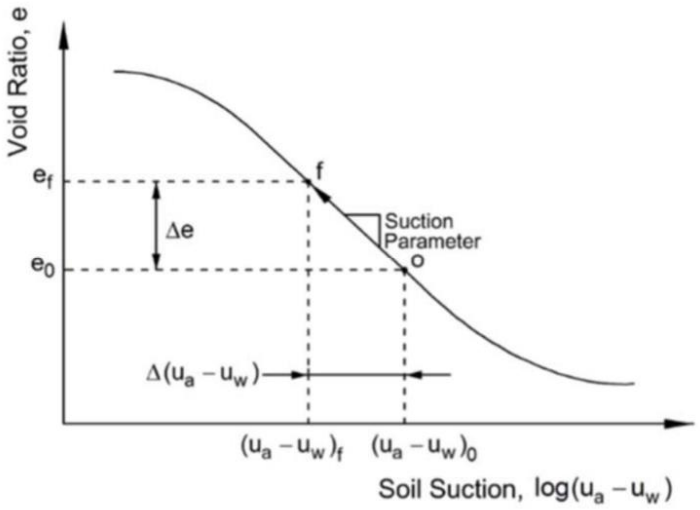

Figure 1.19 Determination of Suction Compression Index from the Void Ratio vs. Soil Suction Plot (Tu 2015)

The suction compression index is defined as the change in volume, or void ratio, related to the change in suction for an undisturbed specimen of soil. (Amer 2016) Suction compression index has been studied by many researchers who created different methods, both empirical and experimental, on how to estimate or calculate γ_h.

1.4.4.2 Methods to Estimate Suction Compression Index, γ_h, Based on Soil Properties

In 1981, McKeen developed a chart, Figure 1.20, based on Activity Ratio, A_C, and Cation Exchange Activity, CEA_c, to calculate the matric suction compression index, γ_h. He defined A_C and CEA_C as,

$$A_c = \frac{PI\%}{\frac{\% - 2micron}{\% - No.200sieve}} \times 100$$

Where,

PI% – the plasticity index in percent; %–2micron – percent of soil particles finer than 2-micron (0.002 mm); and %–No.200 sieve – percent of soil passing sieve #200 (smaller than 0.075 mm).

$$CEA_c = \frac{CEC\,\frac{milli\ equivalents}{100\ gm\ of\ dry\ soil}}{\frac{\% - No.2micron}{\% - No.200\ sieve}} \times 100$$

where,

CEC – the cation exchange capacity in milliequivalents per 100 gm of dry soil.

The cation exchange capacity (CEC) can be measured using a spectrophotometer or it can be estimated using an equation developed by Mojeckwu in 1979.

$$CEC \cong (LL\%)^{0.912}$$

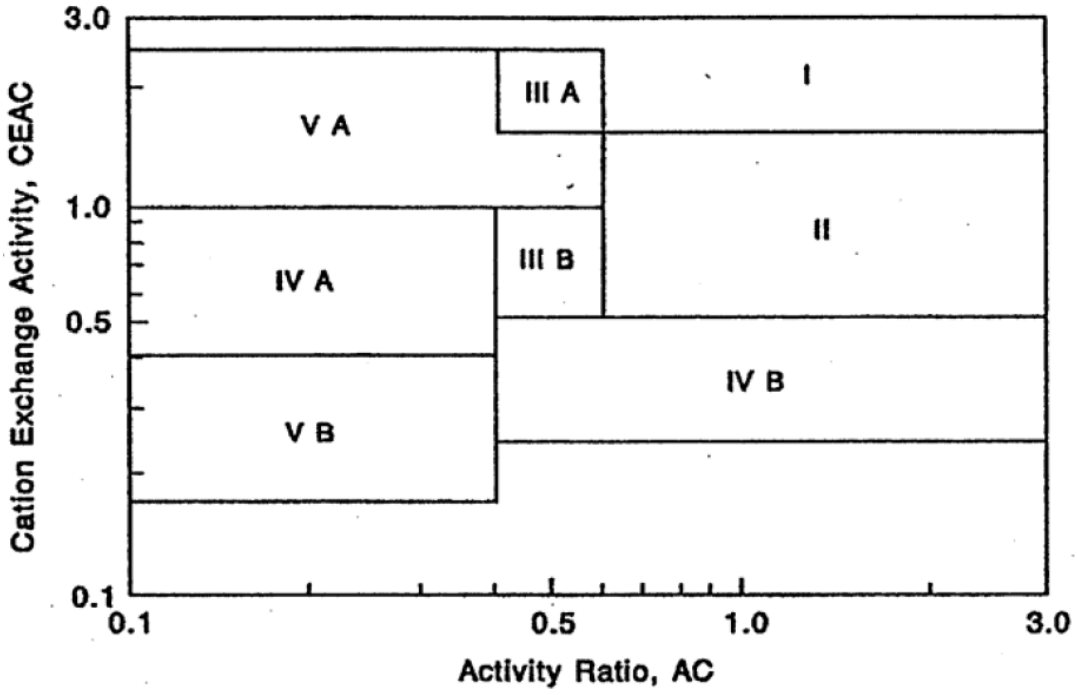

Figure 1.20 Chart for Prediction of Suction Compression Index Guide Number (McKeen 1981)

The regions on the chart each have a volume change guide number corresponding to the suction compression index of a soil with 100 percent fine clay. The values of the guide numbers are given in Table 1.4. The actual suction compression index is proportional to the actual percent of fine clay in the soil. Thus, the actual γ_h is:

$$\gamma_h = \gamma_0 \left[\frac{\% - 2micron}{\% - No.200sieve}\right]$$

Table 1.4 Values for a Soil with 100% Fine Clay Content

Region	Volume Change $\boldsymbol{\gamma_0}$ Guide Number
I	0.220
II	0.163
IIIA	0.096
IIIB	0.061
IVB	0.061
VA	0.033
VB	0.033

1.4.4.3 Estimating Soil Swelling Parameters Based on % Passing No.200 Sieve, %-2micron, LL, and PI

In 2001, Covar and Lytton developed a model to estimate suction compression index simple soil properties (Covar and Lytton 2001). A soil database from the US Department of Agricultural (USDA) Natural Resources Conservation Service (NRCS) was used to collect soil data for more than 40 years. (Lytton 2005) Only soil data containing the following properties were used to develop a new method of obtaining γ_0, liquid limit, plastic limit, plasticity index, percent passing 2-micron, percent passing No. 200 sieve, coefficient of linear extensibility, COLE, and cation exchange capacity.

Partitioning the collected data, about 6400 records, with the Plasticity Chart after Casagrande (1948) and the Holtz and Kovacs (1981) mineral classification chart, the chart is divided into eight different zones based on mineralogical similarity, Figure 1.21.

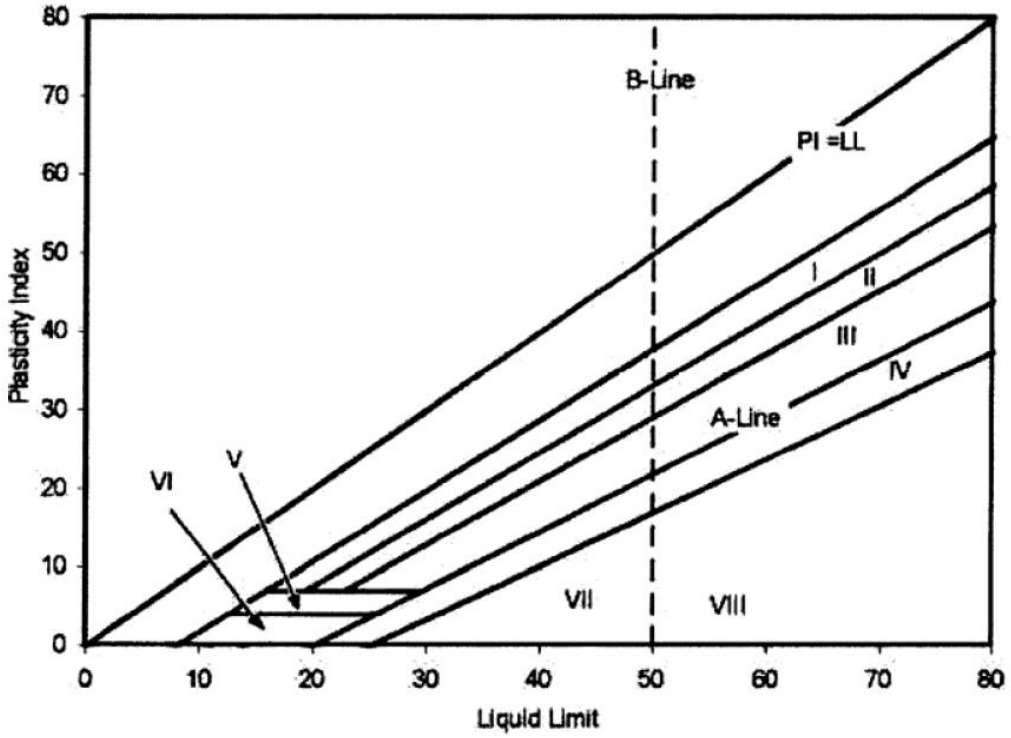

Figure 1.21 Data Filter for Partitioning Database on Mineralogical Types (after Casagrande)

An average matric suction index is calculated for each record using the following equations,

$$\gamma_0\,(swelling) = \left[\left(\frac{COLE}{100}+1\right)^3 - 1\right]$$

$$\gamma_0\,(shrinking) = \left[1 - \frac{1}{\left(\frac{COLE}{100}+1\right)^3}\right]$$

$$\gamma_0(Average) = \left(\frac{\gamma_0\,(swelling) + \gamma_0\,(shrinking)}{2}\right)$$

COLE is determined from a laboratory test, explained in the following section.

Then, $\gamma_0(Average)$ was adjusted to a 100% fine clay content, %fc, where %fc is simply calculated as shown,

$$\%fc = \left[\frac{\% - 2micron}{\% - No.200sieve}\right]$$

And the adjusted suction compression index, γ_h, will be:

$$\gamma_h = \gamma_0(Average).(\%fc) = \left(\frac{\gamma_0\,(swelling) + \gamma_0\,(shrinking)}{2}\right).\left[\frac{\%-2micron}{\%-No.200sieve}\right]$$

Next, for each group of the eight mineralogical groups, γ_0 is plotted as contoured lines on an A_C vs *LL / %fc*. Figure 1.22 shows the graphs for Zone I and Zone II as examples. The rest of the graphs can be found in the original paper, Covar and Lytton 2001. As a result, γ_h can be estimated empirically based on % Passing No.200 Sieve, %-2micron, LL, and PI.

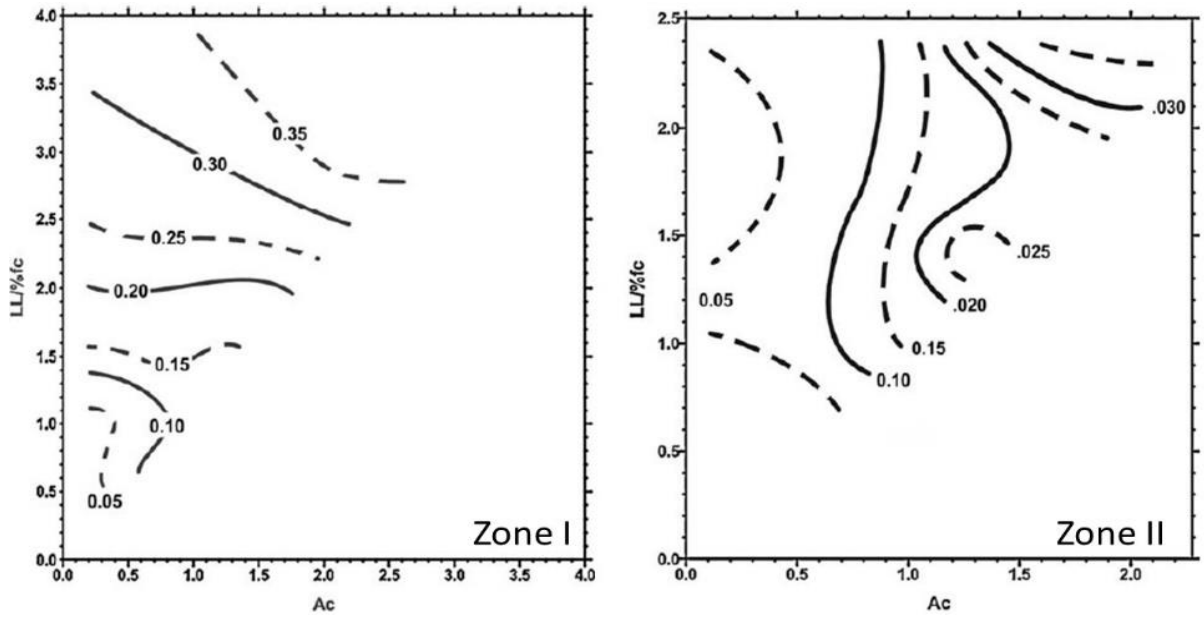

Figure 1.22 Zone I and Zone II Charts for Determining γh

1.4.4.4 Methods to Calculate Suction Compression Index, γ_h, Based on Laboratory Tests

1.4.4.4.1 The COLE Test

Coefficient of Linear Extensibility (COLE) test is a shrinkage test that determines the linear strain of an undisturbed, unconfined sample by drying from 5 psi (33kPa) suction to oven dry suction 150,000 psi (1000 MPa). The procedure starts by coating undisturbed samples with a flexible plastic resin. The resin resist water from entering but allows water vapor to exit. In a pressure vessel, the soil samples, form as clods, are brought to a soil suction of 5 psi. Then, using Archimedes' principle, the volumes are calculated by weighing samples in air and water. Another volume is obtained for the sample after oven dried. Then, COLE can be calculated using the following equation (Amer 2016)

$$COLE = \left[\frac{1}{C_m\frac{(Db_m)}{(Db_d)} + (1 - C_m)}\right]^{1/3} - 1$$

where,

C_m is the Coarse-fragment conversion factor = $\frac{Moist\ volume\ of\ soil\ particles\ less\ than\ 2\ mm}{Volume\ of\ whole\ soil}$; Db_m is the bulk density of the fine-grained soil at 2.52 pF (5 psi) (33kPa); and Db_d is the bulk density of the fine-grained

soil at 7 pF (150,000 psi) (1000 MPa).

If no coarse material exists, the equation is simplified to (Nelson and Miller 1992):

$$COLE = {}^{\Delta L}/_{\Delta L_D} = \left(\frac{\gamma_{dD}}{\gamma_{dM}}\right)^{1/3} - 1$$

where,

${}^{\Delta L}/_{\Delta L_D}$ is the linear strain relative to dry dimensions, γ_{dD} is the dry density of oven dry sample at 7 pF (150,000 psi) (1000 MPa) suction; and γ_{dM} is the dry density of sample at 2.52 pF (5 psi) (33kPa) suction.

The unit pF is the common logarithm of height in centimeters of the water column needed to provide the suction (Schofield 1935):

$$pF = \log_{10} h$$

where,
h is the height of a column of water in centimeters which would give a pressure numerically equal to the suction.

The result of this test is used in an equation proposed by McKeen and Nielsen in 1978 to calculate the suction compression index, γ_h. (Amer 2016):

$$\gamma_h = -\frac{COLE}{log\frac{h_f}{h_i}}$$

where,
h_i is the initial matric suction, pF; and h_f is the final matric suction, pF.

1.4.4.4.2 The CLOD Test

The CLOD test is a modification of the COLE test. Compared to COLE test, the main advantage of CLOD test is that "volume changes are monitored along a gradually varying moisture change path. This results in a smooth shrinkage (or swelling) curve for each sample" (Nelson and Miller 1992). Similar to COLE test, the procedure of CLOD test starts by coating soil samples with resin and measuring the volume. With periodic measurement of volume and weight, samples can dry slowly in room air and temperature until reaching a constant weight. Then, it is oven dried for 48 hours and the final weight and volume is measured.

As a result, a water content, void ratio, and suction relationship can be established. However, this relationship is only valid for water content higher than the soil shrinkage limit because changes in water content are not accompanied by changes in volume below shrinkage limit. This relationship is expressed

in the following equation and Figure 1.23 (Nelson and Miller 1992):

$$C_w = \frac{\Delta e}{\Delta w}$$

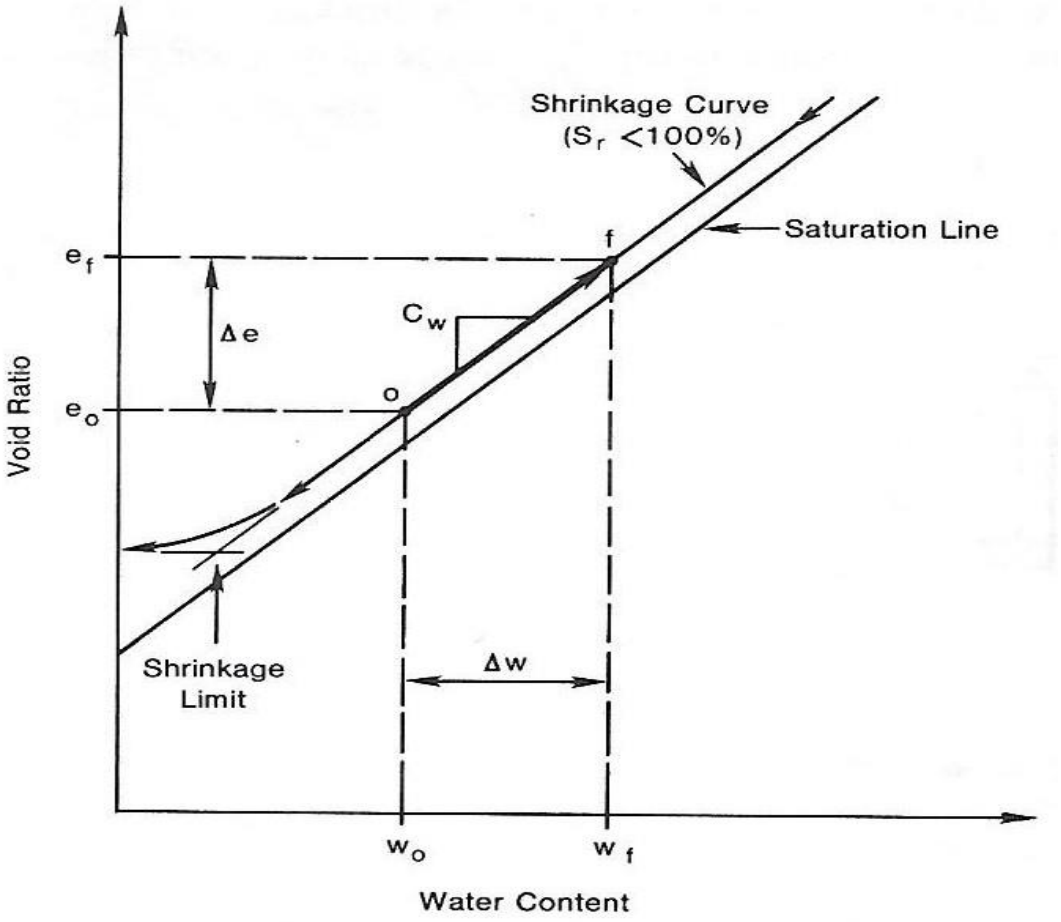

Figure 1.23 Shrinkage Curve in Terms of Void Ratio and Water Content for Determining the Suction Modulus Ratio, Cw (After Nelson and Miller 1992)

where,
C_w is the CLOD index, Δe is the change in the void ratio; and Δw is the change in the water content.

Moreover, heave, Δz_i, can be calculated using the following equations, (Nelson and Miller 1992):

$$\Delta z_i = \frac{\Delta e}{1 + e_0} z_i = \frac{C_w \Delta w}{1 + e_0} z_i$$

And the total heave, ρ, is:

$$\rho = \sum_{i=1}^{n} \Delta z_i = \sum_{i=1}^{n} \frac{C_w \Delta w}{1 + e_0} z_i$$

where,
ρ is the total heave (sum of all increments of heave for each layer). Note that this equation does not consider heave due to effective stress. It is developed based on change in water content and suction.

The Suction compression index, γ_h, can be measured empirically using the following relationship, (McKeen 1992):

$$C_h = -0.02673\left(\frac{\Delta h}{\Delta w}\right) - 0.38704$$

where,
Δh is the change in suction; and Δw is the change in soil water content.

Perko, Thompson, and Nelson conducted CLOD test on 89 relatively undisturbed samples from sites around the Denver, Colorado area to improve McKeen's empirical relationship. The modified equation for the suction compression index based on Perko, Thompson, and Nelson modifications is as follows (Perko, Thompson, and Nelson 2000):

$$\gamma_h = -\frac{10}{3}PL^2\left(\frac{e+F}{e+1}\right)$$

where,
PL is the plastic limit; e is the void ratio; and F is the %-No.200 sieve.

1.4.4.4.3 Volume and Suction Determination Using Digital Imaging

This method was developed by Amer in 2016 where a digital camera was set to capture on frequent basis the volumetric changes of moist undisturbed Shelby tube soil specimen, which was prepared for air-drying shrinkage testing at a temperature-controlled environment, Figure 1.24. The test was stopped when volume change seizes or after 40 hours, minimum. Then, filter paper test was conducted to measure water content and suction of the soil specimen. The main advantages of this method compared to other methods used to estimate or calculate γ_h, according to the author, is "(1) it yields incremental γ_h representative to the entire nonlinearity of the suction-volumetric strain relationship and (2) it is a direct method." (Amer 2016). Other advantages are economical, easy, and relatively fast.

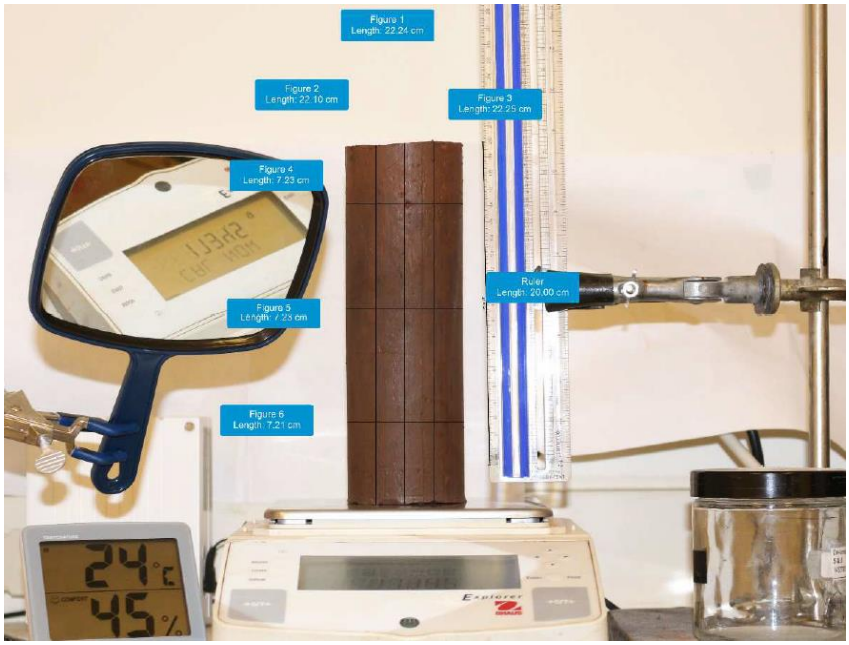

Figure 1.24 Soil Specimen Captured During a Drying Test (After Amer 2016)

1.4.4.4.4 Direct Measurement of the Suction Compression Index via OPPD Testing

Directly measured suction compression indices for expansive clay soil were gathered by Olaiz (2017) using an oedometer pressure plate device (OPPD). The OPPD device developed by GCTS in Tempe, Arizona with the aid of Dr. Delwyn Fredlund, allows for the control and measurement of the matric suction, water content, and deformation of a soil sample. The complete apparatus is shown in Figure 1.25.

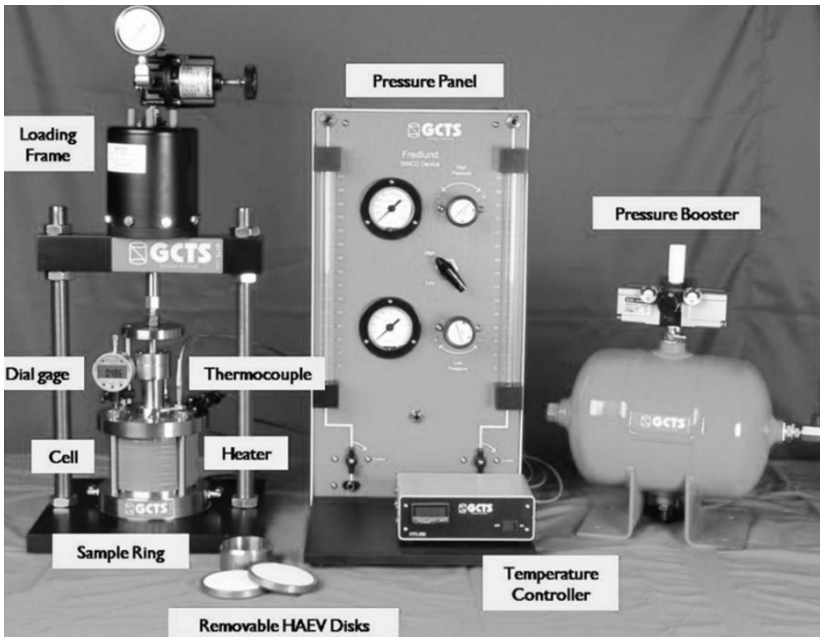

Figure 1.25 Oedometer Pressure Plate Device (OPPD) (GCTS, Tempe AZ)

Olaiz's work improved the testing method for the measurement of the suction compression index using the OPPD; however, he concludes that directly measuring the value is not practical due to the long testing duration, cost, and highly propensity of human and mechanical error (Olaiz, 2017).

1.4.4.4.5 Mean Principal Stress Compression Index

The mean principal stress compression index, γ_σ, can be calculated using its relation to the compression index, C_c, and void ratio, e, as follows (Lytton 2005):

$$\gamma_\sigma = \frac{C_c}{1 + e_0}$$

where,
C_c is the compression index; and e_0 is the void ratio.

The mean principal stress can be calculated using:

$$\sigma = \frac{1 + 2K_0}{3}\sigma_z$$

where,
σ_z is the vertical stress at a point below the surface in the soil mass; and K_0 is the lateral earth pressure coefficient.

$$K_0 = e\left(\frac{1 - sin\emptyset'}{1 + sin\emptyset'}\right)\left(\frac{1 + dsin\emptyset'}{1 - ksin\emptyset'}\right)^n$$

Values of coefficients e, d, k, and n for different soil conditions are given in Table 1.5.

Table 1.5 Values for a Soil with 100% Fine Clay Content

Conditions	K_0	e	d	k	n
Cracked	0	0	0	0	1
Drying (Active)	1/3	1	0	0	1
Equilibrium (at rest)	1/2	1	1	0	1
Wetting (within movement active zone)	2/3	1	1	0.5	1
Wetting (below movement active zone)	1	1	1	1	1
Swelling near surface (passive earth pressure)	3	1	1	1	2

The angle of internal friction, ϕ', can be estimated from its empirical correlation with plasticity index, PI, based on triaxial compression tests (Figure 1.26).

$$\emptyset' = 0.0016PI^2 - 0.3021PI + 36.208$$

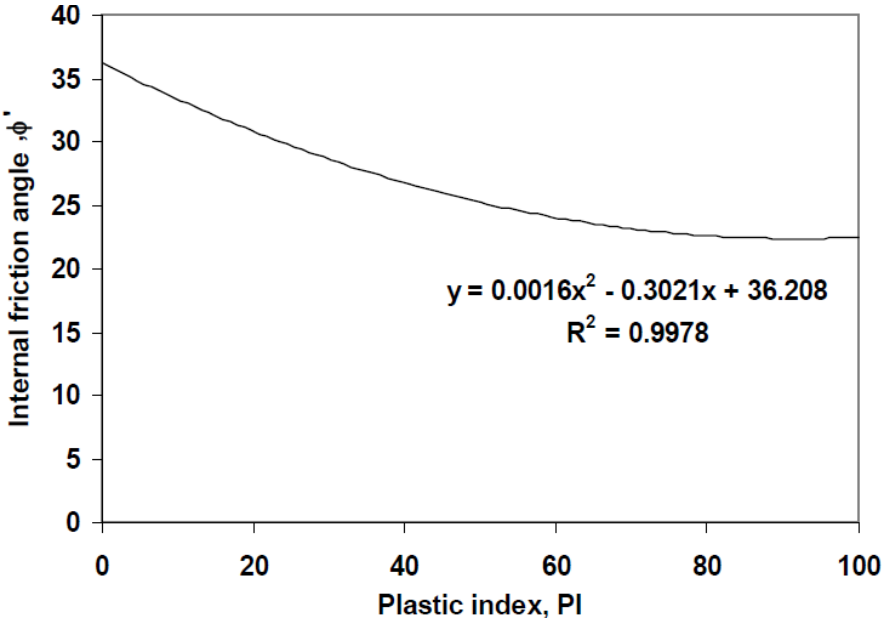

Figure 1.26 The Regression Equation based on the Relation on the Empirical Correlation Betweenϕ' and PI. (Lytton 2005, after Holtz and Kovacs 1981)

The toughest parameter to obtain for the determination of the mean principal stress compression index is the compression index (C_c). The parameter can be obtained via extensive 1-D oedometer testing which involves continuing increasing the net normal stress while measuring the changes in strain. The authors of this study will explore new empirical models, which can determine the mean principal stress compression index based on soil properties and depth within the soil profile.

The study conducted by Rosenbalm in 2013, will aid in the development of the new empirical determination of the mean principal stress compression index. The objectives of Rosenbalm's study were (1) to assess the effects of density and initial water content on the swell pressure of a compacted expansive material that is subjected to multiple wetting and drying cycles and (2) to determine the mechanical behavior and volume change affected by wetting and drying cycles. (Rosenbalm and Zapata 2017). Soils from Anthem, Arizona, and Denver, Colorado, were used. Five or six samples were created for each soil, which were compacted at 90, 100, and 110% of optimum moisture content, OMC, and 90, 95, and 100% of maximum dry density, MDD. Also, five or six compacted specimens were prepared for testing because different net normal stresses were used for each initial compacted condition. Then, each sample was subjected to six wetting and drying cycles and the vertical strain was measured at the end of each cycle. The study concluded that:

- "Four to five wetting and drying cycles are needed to reach equilibrium swell/collapse strain after wetting.
- Two to three wetting and drying cycles are needed to reach equilibrium shrinkage after drying.

- At a particular applied net normal stress, the initial wetting/drying cycle acts as a preconditioning cycle that significantly reorients the soil fabric from the initial compacted condition towards a state of soil-fabric equilibrium.
- Preferred wetting paths were observed within the soil structure due to the vertical and horizontal cracks that formed during the drying process, which expedites the time required to reach primary swell or collapse.
- For applied net normal stresses less than 25% of the swell pressure, the soil undergoes swelling. On the other hand, if the applied net normal stress is greater than 25% of the swell pressure, the soil will collapse.
- The swell pressure was reduced with additional wetting and drying cycles and tends to equilibrate to value around the fifth or sixth wetting/drying cycle. In addition, the initial compacted condition affects the rate at which the swell pressure reduction or vertical deformation increase/reduction occurs; and
- The initial compacted condition of 110% OMC and 90% MDD appears to mitigate most of the swell potential and swell pressure from compacted expansive soil. This initial compacted condition yielded the highest decrease in swell pressure as additional wetting and drying cycles were performed." (Rosenbalm and Zapata 2017).

1.4.5 The Surrogate Path Method for Heave Computation

Singhal (2010) proposed a method for estimation of partial wetting heave in which the suction compression index and mean principal stress compression index need not to be known. Since the procedure estimates the partial wetting strain, without using the suction compression index, it is referred to as the Surrogate Path Method (SPM). The SPM provides a method for mapping the wetting path in the volume change versus log matric suction plane (for a fixed net normal stress) into the volume change versus log net normal stress plane.

The figure below illustrates the 3-dimensional plot of the SPM (Singhal 2010), where the matric suction (u_a-u_w) and vertical strain (ε) axes are arithmetic and the net total stress (σ-u_a) axis is logarithmic.

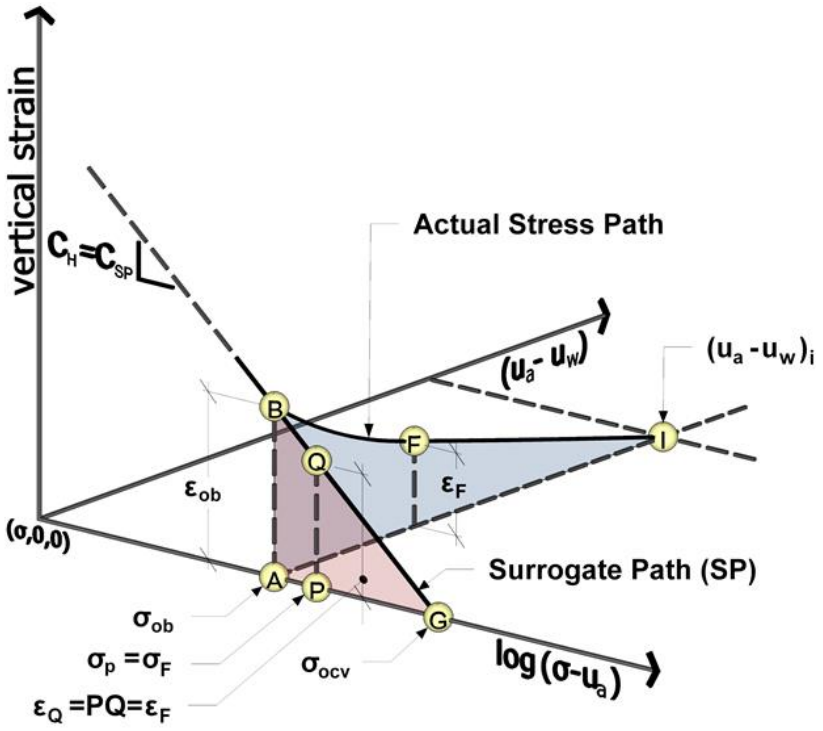

Figure 1.27 Strain-Based "Equivalence" of Reduction of Suction from (ua– uw)i to Zero (Path IB) to Reduction in Net Normal Stress from σOCV to σob (along path GB, the SP)

Houston and Houston (2017) best explain the SPM illustration and procedure as follows. It is important to note that the SPM illustration (**Error! Reference source not found.**) is not necessary for the e stimation of the partial wetting heave if the outlined computation procedure is followed. However, Figure 1.27 is discussed in more detail below.

In Figure 1.27, Point I is depicted as the initial point for the wetting process where the suction is $(u_a\text{-}u_w)_i$. The plane IBA is parallel to the suction axis and perpendicular to the net stress axis. Point B lies in the net total stress plane where the suction is zero (i.e., full wetting). The path (curve) IFB is the suction path for full wetting and produces a full wetting strain, $\varepsilon_{ob} = \varepsilon_{fw}$ (i.e., the strain corresponding to the distance AB in Figure 1.27). The path IFB is labeled as the Actual Stress Path and is curved, not a straight line. IFB would be somewhat non-linear if suction were plotted on a log scale, and it is even more non-linear given that suction is plotted arithmetically. For partial wetting, the matric suction does not go all the way to zero but stops at a final condition demonstrated by Point F where the strain is $\varepsilon_{pw} = \varepsilon_F$.

Now consider this wetting path IFB mapped as path GQB in the σ plane, where $(u_a\text{-}u_w) = 0$. The path GQB is the path for wetting to zero matric suction at Point B. The path BQG is established as follows:
A test specimen with initial suction $(u_a\text{-}u_w)_i$ and field overburden stress of σ_{ob} is loaded in the laboratory oedometer to σ_{ob} and then submerged. When swelling ceases, the strain is ε_{ob}, which plots as AB in Fig. 1.27. Note that where structural loads are significant, the applied stress (referred to here as σ_{ob}) should be overburden plus structural load.

- A second specimen, as nearly identical as possible to the first specimen, is loaded to a higher stress (preferably 2 to 3 times σ_{ob}, or more), then flooded, and the resultant strain is plotted versus the applied stress. Extrapolation (or interpolation) through points B and the second specimen point on the stress axis is used to approximate the swell pressure, σ_{ocv}, at zero strain (point G). This technique has been widely used to approximate σ_{ocv} (Houston and Nelson, 2010). The subscript "ocv" refers to the swelling pressure for a specimen first loaded to overburden and then subjected to a constant-volume swell pressure measurement. Alternatively, the load-back procedure, with correction, can be used to approximate the constant volume swell pressure, σ_{ocv} (Thompson 2006; Nelson et al. 2006).

With σ_{ocv} established at point G, the line GB serves as a surrogate path (SP) for the Actual Stress Path. Note that the actual path IFB generates a full wetting strain of ε_{ob} = AB, and the surrogate path (SP) generates the same strain, ε_{ob}, in going from G to B. The objective of the interpolation method is to find an intermediate stress between σ_{ob} and σ_{ocv}, call it σ_p, that produces a strain PQ that is equal to ε_F, the partial wetting strain at Point F. This interpolation is accomplished by using the proportion of suction dissipated by wetting from I to F as a proportionality factor in estimating the final net stress, σ_p, at point P. In other words, R_w is defined as $R_w = (u_a-u_w)_f / (u_a-u_w)_i$ where $(u_a-u_w)_i$ is the initial suction and $(u_a-u_w)_f$ is the final suction. Thus $R_w = 1$ for no wetting and $R_w = 0$ for full wetting, and $(1-R_w)$ = degree of wetting. Then, $\sigma_p = \sigma_{ob} + R_w (\sigma_{ocv} - \sigma_{ob})$. The actual path, I to F, in Figure 1.27 is replaced with the surrogate path, GQ. The strain PQ at point P (ε_Q) was compared by Singhal (2010) to laboratory suction-controlled measured strain ε_F for numerous cases and an excellent agreement was found for all cases. The SPM interpolation was found to consistently produce results with less than 10% error for heave simulation cases explored by Singhal (2010).

The SPM requires that initial and final suction values in the field be measured or estimated; the SPM does not require that suction-controlled oedometer testing be performed, but rather employs the very familiar oedometer procedure and apparatus. The SPM does not require that the slope of the strain-log suction curve, γ_h, be measured or estimated and problems with the nonlinearity of this curve in the low and high suction range are greatly reduced or eliminated. However, it is noted that the data needed to estimate the suction compression index is readily available from the SPM without measuring or controlling suction. This is because the strain at point F, ε_F, is determined by the SPM and then γ_h in going from $(u_a-u_w)_i$ to $(u_a-u_w)_f$ can be back-calculated, if wanted. However, there is no particular need to make this computation because the strains are readily estimated from the SPM for any value of $(u_a-u_w)_f$ between $(u_a-u_w)_i$ and zero, and the strains are the ultimate objective.

Singhal (2010) points out that one of the strengths of the SPM is that it is founded on the full-wetting oedometer test and is thus forced to be more or less exactly correct at the extremes of no wetting and full wetting. Singhal also found that the SPM results are not very sensitive to the estimate of σ_{ocv}, and therefore, it is acceptable to use corrected load-back values for σ_{ocv}. The SPM is simply used to provide a reasonable, rational method for interpolation between the extremes – which it does. The SPM is a soil-suction-based approach in that it requires estimates of initial and final suction, and in that the proportionality factor, R_w, is computed from numerical values of suction. However, the SPM is actually a marriage of suction-based approaches and the overburden swell test performed in the familiar oedometer

apparatus.

The following summarizes the procedure for the determination of the SPM partial wetting strain (ε_{pw}), in lieu of **Error! Reference source not found.**, as laid out by Houston and Houston (2017). The initial m atric suction $(u_a\text{-}u_w)_i$ of the soil must be known or estimated. The ratio (R_w) of the initial matric suction to the chosen final matric suction is determined as:

$$R_w = \frac{(u_a - u_w)_i}{(u_a - u_w)_f}$$

The slope of the surrogate path (C_{SP}) is then calculated using the fully wetted oedometer strain (ε_{ob}) under the field net normal stress (σ_{ob}) and the load back swell pressure (σ_{cv}).

$$C_H = C_{SP} = \frac{e_{ob}}{\log\left(s_{cv} / s_{ob}\right)}$$

Next, intermediate stress (σ_p) between σ_{ob} and σ_{cv} is determined by:

$$s_p = s_{ob} + R_w\left(s_{cv} - s_{ob}\right)$$

Lastly, the final partial wetting strain is calculated by:

$$e_{pw} = e_f = C_H \log\left(s_{cv} / s_p\right)$$

Houston and Houston (2017) have observed that errors in the estimation of the final matric suction value are dampened by the SPM. For the above example, if the final suction were 200 kPa rather than the estimated 250 kPa, this would represent an error in final soil suction of 20%. If this final suction error is carried through to the computation of final swell strain, the strain becomes 2.83% instead of the computed 2.58% - an error of about 10%.

1.4.5.1 Statistical Evaluation of the SPM

Vann et al. (2018) performed a comparison study of the directly measured strains from the Olaiz (2017) work and those estimated by the SPM using both measured suctions and estimated suctions from the previously discussed suction surrogate, which was proposed in the same study. Table 1.6 summarizes the comparison, which shows great agreement between the estimated strains and the directly measured strains.

This study will incorporate and compare the heave model proposed by Lytton (2005) and the Surrogate Path Method proposed by Houston and Houston (2017).

Table 1. 6 Comparison of Measured and Predicted Partial Wetting Strain (Vann et al. 2018)

Sample ID	$\varepsilon_{OPPD\ MEASURED}$	ε_{SPM}	$\varepsilon_{SPM\ SURROGATE}$	ε_{MOM}
D-1	0.32	0.41	0.32	0.21
D-3	0.94	1.03	0.98	0.65
D-7	0.10	0.16	0.10	0.10
SA-1	0.21	0.26	0.21	0.21
SA-6	0.21	0.24	0.17	0.19
SA-9	0.61	0.53	0.50	0.36
D-8	0.41	0.46	0.04*	0.30
SA-10	0.32	0.39	0.31	0.31
SA-2	0.10	0.12	0.11	0.19
SA-4	0.21	0.26	0.21	0.19
SA-7	0.47	0.36	0.18	0.29
D-9	0.10	0.34	0.28	0.19
SA-11	0.32	0.35	0.28	0.26
SA-3	0.52	0.57	0.50	0.44
SA-5	0.21	0.19	0.18	0.14
SA-8	0.21	0.26	0.23	0.18
D-5	0.21	0.32	0.25	0.19
D-10	0.63	0.51	0.43	0.12
Mean	0.34	0.38	0.29	0.25
σ	0.217	0.201	0.207	0.128

*An error in calculated water content from OPPD manometer is suspected but not verified.

1.5 Models for Frost Heave

When soil is subjected to freezing conditions, the thermal disturbance will lead to changes of physical properties that are indicative of its state variables (i.e., temperature, water contents, and displacements or volume change) and parameters related to soil properties (i.e., thermal, and hydraulic conductivities, and mechanical moduli). Such properties vary during the frost process. Various models have been developed to simulate the variations of soils under the frost effects. The distributions of temperature and water content as well as the associated volume change have been the focus of investigations. Hydrodynamic models and rigid ice models are two of the most common types of models for this purpose. Examples of models that consider frost effects are presented in this section.

1.5.1 CRREL Model

The effects of frost penetration in the Pavement ME Guide (EICM) are originally based on the CRREL model, which is a one-dimensional model for heat and moisture transport in the vertical direction. The primary research objectives of this CRREL study dealt with models associated with both Frost Heave and Thaw Settlement. The thermal/moisture modelling equation was originally solved with nodal domain integration method but can also be solved with finite difference or finite element method. The model is

based on the following assumptions (Guymon et al. 1986):

4. Moisture transport in the unfrozen zone is governed by the unsaturated flow equation based upon continuity and Darcy's law.
5. Moisture flow is by way of liquid movement and vapor flow is negligible.
6. Moisture flow in the frozen zone is negligible and there is no moisture escape or addition at the frozen soil surface.
7. Soil deformations in the unfrozen zone are negligible.
8. Soil pore water pressures in the freezing zone are governed by an unfrozen water content factor.
9. All processes are single valued, i.e., there is no hysteresis.
10. Heat transport in the entire soil column is governed by the sensible heat transport equation, including an advective term.
11. Salt exclusion processes are negligible, i.e., the unfrozen water content is constant with respect to temperature.
12. Phase change effects and moisture effects can be modeled as decoupled processes.
13. Freezing or thawing can be approximated as an isothermal phase change process.
14. During thawing, settlement in the thaw zone is dominant and consolidation effects are negligible.
15. Constant parameters are invariant with respect to time.
16. All parameter and model uncertainty can be incorporated into a universal probability model applicable to a specific class of soils.

Advantages of this model include:

- Formulation is in 1D form, which can be conveniently solved with several numerical methods such as the nodal domain integration method, the finite difference method, the integrated finite difference method, finite element method, or any other mass lumping numerical method.
- Included ‘convective’ or ‘advective’ term of the heat equation, which significantly improves the estimation of frost heave.
- Included the gravity term, which makes it perform better for very moisture soils or thawing ice-rich soils where the gravity plays an important role.

Limitations include:

- The model was primarily validated for non-cohesive frost-susceptible soils with grain sizes ranging from silts to dirty gravels. Extreme technical difficulties were found when the approach was used on clay soils of varying PI values.
- Ice segregation potential and overburden effects are not properly accounted for. i.e., the model is applicable for small overburden pressure.
- The effects of solutes are not considered and therefore, it is applicable for situations with low salt content. Increasing salt concentration decreases heave according to Cary (1987).
- Frost heave is estimated as a lumped quantity that is equal to the total ice segregation in the frozen zone. The expansion of soil matrix is not considered. This can lead to errors in the frost heave estimation.

- To facilitate the solution of the hydraulic problem, a characteristic negative value water pressure is assumed at the top of a freezing element (decided by the unfrozen water content), which approach zero water pressure by an amount corresponding to the overlaying pressure (due to moisture migration). This has the effect of reducing the calculated rate of frost heave.
- The procedures to solve the thermal problem led to an increase in the rate of heat transfer through the zone of freezing and lead to an increase in the rate of penetration of the frost.

1.5.2 Hydrodynamic Model

The hydrodynamic models cover the various models developed by soil physicists to predict the water and temperature redistribution in unsaturated soils. Most of these models are Thermo-Hydraulic (TH) models. Engineers in the geotechnical engineering community are making efforts to establish Thermo-Hydro-Mechanical (THM) models by importing the TH framework (Nishimura et al. 2009; Thomas et al. 2009). The characteristic of these models is that the ice pressure is usually assumed to be zero or the changes in the ice pressure is ignored. This assumption is seldom questioned except in cases such as ground heaving where such assumptions might be invalid (Miller 1973; Spaans and Baker 1996; Hansson et al. 2004).
One TH model widely referenced is the coupled heat-fluid transport model developed by Harlan (1973). The key factors for this coupled model include the analytical expression for the Gibbs free energy (equivalent to SWCC), which was assumed to establish a unique relationship between soil-water potential and liquid water content, and the similarity between a freezing and a drying process (Harlan 1973, i.e., Eqs. below. The original one-dimensional equation system in Harlan (1973) is written in three-dimensional forms here.

$$\frac{\partial(\rho_w C_a T)}{dt} = \nabla(\lambda \nabla T) - \rho_w C_a \nabla(\frac{\vec{J}}{\rho_w} T)$$

$$\frac{d(\rho_w \theta_w)}{dt} + \frac{d(\rho_i \theta_i)}{dt} = \nabla(\frac{K}{g} \nabla \psi)$$

Where,
θ_i is the volumetric ice content and ρ_i is the density of ice. Previous equations present a coupled hydrodynamic model.

As pointed out above, θ_l is a function of Gibbs free energy ψ (definition of SWCC). Besides, the change in ice per unit volume per unit time is re-written as the function of ice content.

Later researchers such as Guymon and Luthin (1974) confirmed that soil moisture and thermal states were coupled, particularly during freezing and thawing processes. Based on this, models similar to Harlan's model were developed. The differences are in the different correlations used to fit the relationships between parameters such as the hydraulic conductivities and other independent variables. Guyman and Luthin (1974) estimated ice content by an empirical relationship suggested by Nakano and Brown (1971) instead of combining SWCC and the Clapeyron equation. Other researchers, e.g., Taylor and Luthin (1978), Jame and Norum (1980), Hromadka and Yen (1986), Noborio et al. (1996a), Newman and Wilson (1997) and Hansson et al. (2004), established slightly different models that can be regarded as

modifications to Harlan's model. For example, Hansson et al. (2004) model use the same governing equation form except vapor terms were considered. These modifications over Harlan's model mainly updated the models by using updated relationships and numerical strategies (Celia et al. 1990). Results of simulations compared well with experimental results (Mizoguchi 1990).

There are different choices in the use of water content or pressure as the independent variable. Dirksen and Miller (1966) favored the pressure type Richards' equation because flow could be contrary to water content gradient but would not be contrary to pressure/tension gradient. Celia et al. (1990) showed that the mixed type Richards equation was useful because of its advantage in avoiding large errors in mass balance that the pressure type model usually resulted in.

1.5.3 Rigid Ice Model (Miller type)

A large amount of research has been conducted on frost heave since the late 1970s. This kind of problem cannot be described by applying the governing equations in thermodynamic model directly, due to the existence of an ice lens. The Rigid ice model is proposed, which assumes that ice pressure is not necessarily zero.

The Miller type of rigid ice model is an extension to thermodynamic models with a nonzero ice pressure. The breakthrough of Miller's model lies in the dependence of ice pressure on a new term: the mean curvature (Miller 1978). With relationships derived from this dependency, ice lens initiation can be investigated by analyzing the force balance as follows:

$$\frac{\partial(\rho_w C_a T)}{\partial t} + \frac{\partial(\rho_w L_f \theta)}{\partial t} = \nabla(\lambda \nabla T)$$

$$\nabla \vec{J}_l = \left[\rho_i v_i + \frac{(\rho_l - \rho_i)}{\rho_i} \vec{J}_i \right] \nabla\theta$$

where,

v_i is the rate of frost heave.

Miller (1980) applied the model to simulating very simple quasi-static state with a simplified set of equations. O'Neill and Miller (1985) provided a strategy for obtaining numerical solutions of the full set of equations for simple boundary conditions. The physical basis of the formulation, mathematical expression and implementation was expanded by O'Neill and Miller (1985).

Gilpin (1980) introduced a quasi-static strategy to solve the coupled model. Aiming at an overall prediction but with local information obtained by continuum mechanics, the author divided a freezing sample into frozen zone, frozen fringe and unfrozen zone. Solution was obtained by ensuring the energy and mass balance across individual zones. The model succeeded in explaining the formation of discreet ice lenses and predicting the rate of frost penetration and extent of frost heave. The idea of this model was referenced by subsequent researchers in frost heave research, i.e., Sheng et al. (1995).

1.5.4 Semi-Empirical Model

Semi-empirical models were proposed by Konrad and Morgenstern (1980, 1981, 1982a) and received significant attention between 1980s and early 1990s. These models start from a practical standpoint to provide good predictions that match the experimental observations. The role of ice pressure was negligible in the original model (Konrad and Morgenstern, 1980, 1981) and ice pressure was introduced later for considering the effects of applied pressure on freezing soils (Konrad and Morgenstern 1982b).

These models, which had been calibrated from experimental data, have allowed for engineering frost-heave calculations (Kujala 1997). For example, these models were extended for applications such as estimation of frost heave beneath pipelines (Nixon 1991). This assumed that the rate of heaving (water intake velocity) was directly related to the temperature gradient at the frost front in either steady state (Konrad and Morgenstern, 1981) or transient state (Konrad and Morgenstern 1982a). The corresponding proportionality was called segregation potential. The segregation potential was treated as an important property for characterizing a freezing soil. The segregation potential depends on pressure, suction at the frost front, cooling rate, soil type, and so forth (Nixon 1991). Frost heave can be calculated once the segregation potential and other parameters such as temperature gradients are available. The mathematic representation of the segregation potential is given by:

$$SP(t) = \frac{v_{\mathrm{w}}(t)}{\nabla T(t)}$$

where,

SP is the segregation potential, v_{w} is the water intake velocity, and ∇T is the temperature gradient at the frost front. All the three quantities are functions of time.

1.5.4.1 Poromechanical Model

The development of poromechanics offers a new perspective of modeling geomaterials such as soils exposed to freezing conditions. Poromechanics was developed from Biot's theory of dynamic poroelasticity (Biot 1941), which gives a complete and general description of the mechanical behavior of a poroelastic medium. One representative poromechanical model was developed by Coussy (2005) and Coussy and Monteiro (2008). The dependency of saturation and temperature at freezing temperature was obtained by upscaling from the elastic properties of the solid matrix (Dormieux et al. 2002), pore access radius distribution, and capillary curve. It also features the advantage that the microscopic properties are linked to the bulk properties such as bulk modulus, thermal volumetric dilation coefficient of the solid matrix. The original Biot's theory consists of four distinct physical constants accounting for the mechanical properties (Biot and Willis 1957). Coussy (2005) and Coussy and Monteiro (2008) introduced other parameters to account for the ice formation and thermal expansion, which can be reduced to four independent parameters. The micro-macro relationships extended from Biot's coefficients are listed as:

$$b_{\mathrm{C}} + b_{\mathrm{L}} = b = 1 - \frac{K_{\mathrm{S}}}{k_{\mathrm{S}}}$$

$$\frac{1}{N_{jj}} + \frac{1}{N_{LC}} = \frac{b_j - \Phi_0 S_j}{k_S}$$
$$a_j = \alpha_S (b_j - \Phi_0 S_j)$$

where,

K_S is the drained bulk modulus, b and N are the Biot coefficient and the Biot modulus respectively, a_j is the thermal volumetric dilation coefficient of the true porous solid. These macroscopic properties are linked to the bulk modulus of solid particles, k_S, and the thermal volumetric dilation coefficient of the solid matrix, α_s. Φ_0 is the initial Lagrangian porosity and j is a dummy index for phase j, The subscript *C* and *L* indicate solid and liquid phases respectively. The generalized Biot coupling moduli N_{jk} satisfy the Maxwell symmetry relations: $N_{LC} = N_{CL}$.

This poromechanical model provides comprehensive quantitative predictions for the mechanical behavior while accounting for the multi-scale physics of the confined crystallization of ice. The constitutive relationship of Coussy's poromechanical theory was developed from Biot's general theory of consolidation (Biot, 1941). Therefore, the model accounted for the existence of air bubbles. However, Coussy used the term "unsaturated" to stress the difference between this air-entrained state and a full saturated state which was adopted in Power's model (1950). This modification was based on the fact that Power's model (Power 1950) may lead to unrealistic prediction of pressure and shrinkage by neglecting the entrained air bubbles. With the assistance of poroelasticity, volume change attributed to a different mechanism can be analyzed with the constitutive relation. It must be noted that theoretical extension from saturated condition to unsaturated condition for mechanical field is still far from well developed, though several methods based on experiment are available (Alonso et al. 1990; Lu and Likos 2006). Some other challenges of poromechanical models include information about the porous media such as the morphology and surface chemistry of constituents, which are difficult to obtain and formulate.

1.5.4.2 Other Models

There are other types of models such as the thermomechanical models (Duquennoi et al. 1989; Fremond and Mikkola 1991; Li et al. 2000, 2002). As summarized in Li et al. (2002), the thermomechanical modeling by Fremond and Mikkola (1991) took the deformation factors and the phase-changing behaviors into account. The behaviors of the thermal-moisture induced deformation of freezing soils were described using the mechanical theory of mixtures in these models.

1.6 The Effects of Frost Heave on Pavement Ride Quality

Frost heave affects pavement performance by causing serious damage to the pavement structure (Schaus et al. 2011; Janoo and Berg 1990; Dore 2002; Roy et al. 1992; Dore et al. 1997). The resulting cracks, dips, heaving, and potholes make diving uncomfortable, damage vehicles and increase the risk of car accidents (Dore et al. 2001). It is costly and takes a huge amount of highway budgets to repair the damaged pavement. Three basic factors work together to generate frost heave: 1) freezing temperatures; 2) frost susceptible soils (such as silty soils or clayey soils); 3) water in the subgrade soils (Oswell 2011). Frost heave of soils is a complex coupled multi-physical process involving the coupling of the thermal-

hydro-mechanical (THM) field (Li et al. 2000; Neaupane and Yamabe 2001; Liu et al. 2012; Zhou and Meschke 2013; Zhang and Michalowski 2015). The THM process is coupled by extension of soil mechanics under isothermal conditions to incorporate the effects due to thermal expansion of solid skeleton as well as the pore fluid migration (Rabin and Steif 1998; Brownell et al. 1977). The frost heave is the resultant of volume expansion associated with the phase transition of water to ice (around 10% increases in the volume). When subjected to sudden freezing, most soil water freezes without having time to travel large distances. Therefore, the total soil volume expansion is dependent upon the degree of saturation of soil water, or if the pore space is sufficient to accommodate the volume expansion by freezing pore water.

When subjected to slow freezing process, the cryogenic suction drives soil water to migrate toward the ice front, which forms ice lenses. Under such conditions, the volume expansion of soil is significantly affected by the formation of ice lenses and overlain pressure. The first widely accepted theory for explaining the ice lens formation is the capillary theory, which states that water is drawn by the matric suction upwards to form the ice lenses (Taber 1930). The drawback for the capillary theory is that it could not account for the initiation of new ice lenses. Another model to explain the ice lens formation is the frost fringe model, which proposes that frost heave can occur after ice has formed a frozen fringe by penetrating the pores of the soil (Miller, 1972). The particle-engulfment model and geometrical supercooling model are recently developed models to simulate the periodic formation of ice lenses that were observed in the experiment (Mutou et al. 1998; Style et al. 2011).

The amount of frost heave due to ice lens has commonly been estimated by using the segregation potential:

$$\Delta h = 1.09 \cdot SP \cdot \nabla T \cdot \Delta t$$

where,
Δh is the incremental heave over time Δt, ∇T is the temperature gradient in the vertical direction, SP is the soil segregation potential, and the factor 1.09 reflects the volume expansion by around 9% when water freeze into ice.

The rate of heave can also be estimated by empirical methods such as that by Kaplar 1974 in Figure 28.

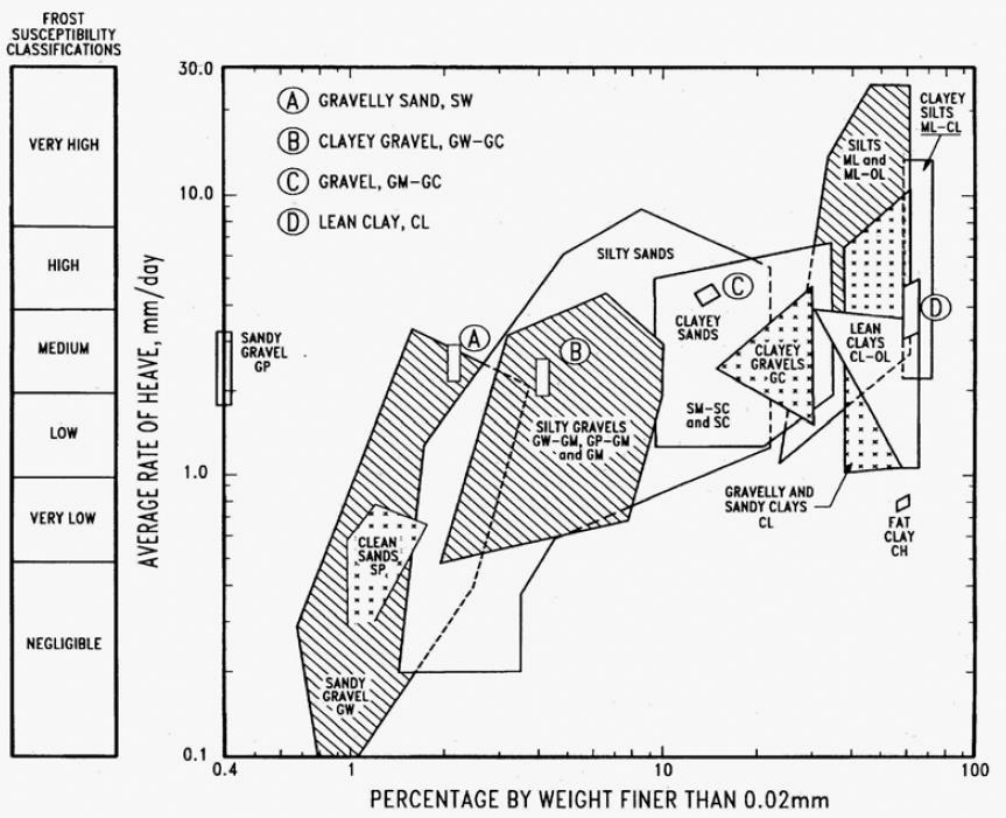

Figure 1.28 Average Rate of Heave versus % Fines for natural Soil Gradations (Kaplar 1974)

Methods for mitigating the frost heave in pavement include increasing the thickness of the base layer that are less susceptible to the influence of freezing/thawing process, thermally insulating the subgrade soil or base layer, and reducing the water content in subgrade soils by good drainage design, etc. (Mackay et al. 1992; Dore et al. 1999). In the engineering design aspect, frost heave is an important format of environmental load that affects ride quality on pavement, i.e., the pavement IRI number.

1.6.1 Serviceability and Roughness

There are four approaches used to evaluate pavement: surface condition or distress, serviceability or roughness, structural capacity, and surface friction (Huang 2004). In this section, the focus is on the serviceability, or sometimes referred to as roughness. Serviceability is the ability of a pavement to perform its intended functions of safety and smoothness at a particular point in time. Roughness, in contrast, is defined by elevation variations existing in the pavement that cause vibrations in vehicles. (Huang 2004; Sandra 2013). A newly constructed pavement has an initial roughness due to built-in surface irregularities, some small level differences that increase with time due to traffic and environmental aspects. Currently, there are two different variables to quantify roughness or serviceability: Present Serviceability Index (PSI), and International Roughness Index (IRI).

1.6.1.1 Present Serviceability Index (PSI)

PSI ranges from 0, that represents a totally impossible road to navigate, to 5, which represents a perfectly smooth road. The design philosophy of the original AASHTO Design Guide was the serviceability-

performance concept, which provided a means of designing a pavement based on a specific total traffic volume and a minimum level of serviceability (called the terminal serviceability) desired at the end of the performance period (AASHTO 1993). Values of Terminal Serviceability Levels, p_t, are selected based on the maximum endurance of pavement before rehabilitation, resurfacing, or reconstruction is necessary. The value of p_t = 2.5 is suggested for major highways and 2.0 is suggested for less traffic highways and major roads. New constructed pavements have initial serviceabilities, p_0, that ranges from 4.5 for rigid pavements to 4.2 for flexible pavements (AASHTO 1993).

1.6.1.2 International Roughness Index (IRI)

The International Roughness Index, IRI, was first presented in the International Road Roughness Experiment in Brazil in 1982. The guidelines for conducting and calibrating roughness measurements were published by the World Bank, the sponsor, and IRI was adopted as a standard for the FHWA Highway Performance Monitoring System (PMS) data base (Huang 2004).

IRI is basically a roughness scale based on the response of a generic motor vehicle (Quarter car model). It is the cumulative vertical deviations over a section of road per unit length, inches/mile for example. Since the original AASHO Road Test, a wide range of roughness measuring devices have been developed. Usually, those devices are connected to vehicles, such as the K. J. Law Profilometer, and measure the vertical acceleration as the vehicle moves over a section of the road. Then, the acceleration is integrated twice to find the displacement. Typical values of IRI are approximately 25-40 in/mile for smooth pavements, and 250-480 in/mile for rough pavements. IRI is evaluated by increments as follows, (Huang 2004):

$$IRI = IRI_0 + \Delta IRI$$

Where,
IRI_0 – smoothness of a new constructed pavement; and ΔIRI is a function of effect of surface distress, D_j, and effect of non-distress variables or site factor, S_f.

A summary of the current Pavement ME Design equations for the IRI and SF, along with the associated regression model coefficients (Ci) for the five major types of new and rehabilitated pavement types are presented below:

Equation for New HMA Pavements and HMA Overlays of Flexible Pavements

$$IRI = IRI_0 + 0.0150(SF) + 0.400(FC_{Total}) + 0.0080(TC) + 40.0(RD)$$

where,
IRI_0 is the Initial IRI after construction (in/mi), *SF* is the Site factor, and the FC_{Total} is the Area of fatigue cracking (combined alligator, longitudinal, and reflection cracking in the wheel path) (% of the total lane area). All load related cracks are combined on an area basis. That is, the length of the cracks is multiplied by 1 ft to convert length into an area basis; *TC* is the Length of transverse cracking (including the reflection of transverse cracks in existing HMA pavements) (ft/mi), and *RD* is the Average rut depth (in).

The site factor (SF) is estimated as follows (Perera and Al-Rawashdeh 2017):

$$SF = Age^{1.5}\{ln[(Precip + 1)(FI + 1)p_{02}]\} + \{ln[(Precip + 1)(PI + 1)p_{200}]\}$$

where,
Age is the pavement age (yr), *PI* is the Plasticity Index of the soil (%), *FI* is the Average annual freezing index (°F days), *Precip* is the Average annual precipitation or rainfall (in), p_{02} is the Percent passing the 0.02 mm sieve, and p_{200} is the Percent passing the 0.075 mm sieve.

Equation for HMA Overlays of Rigid Pavements

$$IRI = IRI_0 + 0.00825(SF) + 0.575(FC_{Total}) + 0.0014(TC) + 40.8(RD)$$

The *SF* is calculated in accordance with the following equation.

$$SF = Age[0.02003(PI + 1) + 0.007947(Precip + 1) + 0.000636(FI + 1)]$$

Equation for Jointed Plain Concrete Pavements (JPCP)

$$IRI = IRI_0 + 0.8203 \cdot CRK + 0.4417 \cdot SPALL + 1.4929 \cdot TFAULT + 25.24 \cdot SF$$

where,
CRK is the Percent slabs with transverse cracks (all severities), *SPALL* is the Percentage of joints with spalling (medium and high severities), *TFAULT* is the Total joint faulting accumulated per mile (in), and *SF* is the Site factor, which is calculated in accordance with the following equation:

$$SF = AGE\ (1 + 0.5556 \cdot FI)(1 + P_{200}) \cdot 10^{-6}$$

where,
AGE is the pavement age (yr), *FI* is the Average annual freezing index (°F days); and p_{200} is the Percent passing the 0.075 mm sieve.

Equation for Continuous Reinforced Concrete Pavements (CRCP)

$$IRI = IRI_0 + 3.15 \cdot PO + 28.35 \cdot SF$$

where,
PO is the Number of medium- and high-severity punchouts/mi, and *SF* is the Site factor, which is calculated in accordance with the following equation:

$$SF = AGE\ (1 + 0.556 \cdot FI)(1 + P_{200}) \cdot 10^{-6}$$

1.7 Summary of Statistical Moments and Probability Distributions

The statistical moments, and statistical distributions used in this study are summarized herein. The descriptions of the statistical moments, hypothesis testing, and statistical distributions are referenced from Fenton and Griffiths (2008), Montgomery et al. (2009, 2011), and Benjamin and Cornell (2014).

The notation used for the mean, standard deviation, and variance depends on the sample size and how representative that sample is to the true population. In this study, the notation representing the population adopted for simplicity is as follows:

- the sample mean ($\bar{x}$) is assumed to represent the population mean (μ)
- the sample standard deviation (s) is assumed to represent the population standard deviation (σ)
- and the sample variance (s^2) is assumed to represent the population variance (σ^2)

Furthermore, subscripts can be added to each of the variables to further denote what population the variable represents.

There are four statistical moments that are used to describe any distribution: mean, variance, skewness, and kurtosis. The mean and variance are heavily utilized in stochastic analyses and are defined herein. are parameters used to further define the shape of the distribution. The standard deviation and the coefficient of variation (*CV*) are also defined.

The first statistical moment is referred to as the expected value ($E[X]$), or the mean value (μ).

$$E[X] = \mu = \left(\frac{1}{n}\right)\sum_{i=1}^{n} x_i \tag{1-1}$$

Where: n = Number of point estimations and x_i = The ith observation of the random variable (x).

The second statistical moment is used to describe the scatter or dispersion in the data and is referred to as the variance ($E\left[X^2\right]$ or σ^2).

$$E\left[X^2\right] = \sigma^2 = \left(\frac{1}{n}\right)\sum_{i=1}^{n}\left(x_i - \mu\right)^2 \tag{1-2}$$

The standard deviation (σ) is defined by the positive square root of the variance and is in the same units as the random variable.

$$\sigma = \sqrt{\sigma^2} \tag{1-3}$$

The standard deviation can be used to define a range of data within a distribution. For example, Figure 1.29, depicts the percentage of a normal distribution represented by number of standard deviations from the mean.

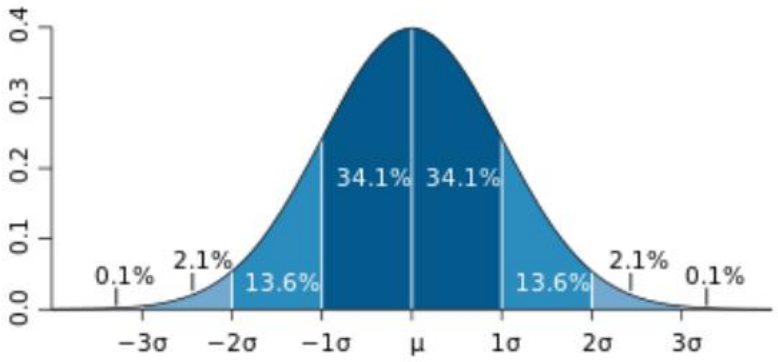

Figure 1.29 Percentage of normal distribution represented by number of standard deviations from the mean.

In a normal distribution, 66.6% (2/3) of the data is represented by 1 standard deviation away from the mean (-1σ to $+1\sigma$); and 95% of the data is represented by 2 standard deviations away from the mean (-2σ to $+2\sigma$). Six standard deviations (6σ) is often referred to as the width of the normal distribution due 99.73% of the data being represented by 3 standard deviations away from the mean (-3σ to $+3\sigma$). The coefficient of variation (*CV*) is defined by the ratio of the mean to the standard deviation.

$$CV = \frac{\sigma}{\mu} \tag{1-4}$$

The third and fourth statistical moment are referred to as skewness and kurtosis. The skewness represents how the mean of the distribution differs from a theoretical mean representing a normal distribution. Kurtosis helps define how much data is dispersed around the mean. The skewness and kurtosis are expressed in the following equations, respectively.

$$E\left[X^3\right] = \left(\frac{1}{n}\right)\sum_{i=1}^{n}\left(\frac{x_i - \bar{x}}{\sigma}\right)^3 \tag{1-5}$$

$$E\left[X^4\right] = \left(\left(\frac{1}{n}\right)\sum_{i=1}^{n}\left(\frac{x_i - \bar{x}}{\sigma}\right)^4\right) - 3.0 \tag{1-6}$$

Continuous random numbers are most often represented using a normal distribution. The normal distribution, or the "Gaussian" distribution, follows a bell curve that is centered about the mean. The variance describes how dispersed or tight the tails of the distribution are from the mean. The probability density function (PDF) represents the shape of probability distributions. The PDF of the normal distribution is expressed as:

$$f\left(x\right) = \frac{1}{\sqrt{2\pi\sigma^2}} e^{-\frac{(x-\mu)^2}{2\sigma^2}} \quad \text{for} \quad -\infty < x < \infty \tag{1-7}$$

The normal distribution is not bound between any values (i.e., the left tail of the distribution will approach negative infinity and the right tail of the distribution will approach positive infinity). As such, issues can arise when generating random numbers for data sets which represent percentages or index values that must be greater than 1 because there is a possibility of producing negative values. This scenario is applicable to the required soil index properties of PI, LL, p200, and pClay as each parameter is

a percentage greater than 0%. The PI and LL parameters do not have an upper bound value but p200 and pClay cannot be greater than 100%. Furthermore, PI is computed from LL and pClay is a fraction of p200 (i.e., must be less than), resulting in high correlation between the parameters, which is discussed further herein. Albeit these limitations for application in stochastic analyses with natural soil properties, the normal distribution is still used as effective tool for preliminary screening of normality for input variable and residuals of regression fits.

For scenarios where the data may be normally distributed but must be greater than zero, a lognormal distribution can effectively represent the data. If a continuous distribution is flexible and bounded on each end with a minimum and maximum value, the Beta distribution can be useful. The basic form of the Beta distribution is defined on an interval [0,1] with two shape factors, denoted as alpha (α) and beta (β), which will be referred to as the "Two-Parameter Beta Distribution" for clarity.

$$f\left(x;\alpha,\beta\right)=\frac{1}{B\left(\alpha,\beta\right)}x^{\alpha-1}\left(1-x\right)^{\beta-1}\ \ for\quad 0\le x\le 1\quad \&\quad \alpha,\beta>0 \tag{1-8}$$

Where:

$$B\left(\alpha,\beta\right)=\frac{\Gamma\left(\alpha\right)\Gamma\left(\beta\right)}{\Gamma\left(\alpha+\beta\right)} \tag{1-9}$$

and Γ = the Gamma function expressed as,

$$\Gamma\left(n\right)=\left(n-1\right)! \tag{1-10}$$

For "Two-Parameter Beta Distribution" with random variable (x), the mean and variance are expressed in terms of the shape factors alpha and beta:

$$\mu_x=\frac{\alpha}{\alpha+\beta} \tag{1-11}$$

$$\sigma_x^{\ 2}=\frac{\alpha\beta}{\left(\alpha+\beta\right)^2\left(\alpha+\beta+1\right)} \tag{1-12}$$

The ability of the Beta distribution to take on many shapes while staying within the defined limits makes it ideal for practical applications. If both shape parameters are greater than one ($\alpha > 1$ & $\beta > 1$), the distribution will be bell-shaped, with the skewness to the right if alpha is less beta ($\alpha < \beta$) or to the left if alpha is greater than beta ($\alpha > \beta$), and with the *mode* representing the peak of the density expressed as:

$$mode=\frac{\alpha-1}{\alpha+\beta-2}\quad for\quad \alpha,\beta>1 \tag{1-13}$$

Beta distributions meeting this criterion with a left-sided skewness can resemble a lognormal, Gamma, Weibull, or Rayleigh distributions. If alpha is less than one, and beta is greater than one ($\alpha < 1$ & $\beta > 1$), the distribution will be "J-shaped" with the *mode* = 0 and the tail heading towards one. Contrary, if alpha is greater than one, and beta is less than one ($\alpha > 1$ & $\beta < 1$), the distribution will be "J-shaped" with the *mode* = 1 and the tail heading towards zero. Beta distributions that are "J-shaped" with *mode* = 0 resemble

an Exponential distribution. However, recall that the Beta distributions are bounded by the specified minimum and maximum values, and the shapes can be flipped if needed the data requires it to be so. An example of this is depicted Figure 1.30 with the shape of the distribution with α = 1 and β = 3 appearing similar the shape of an Exponential distribution, and the shape of the distribution with α = 5 and β = 1 being very similar but in the opposite direction.

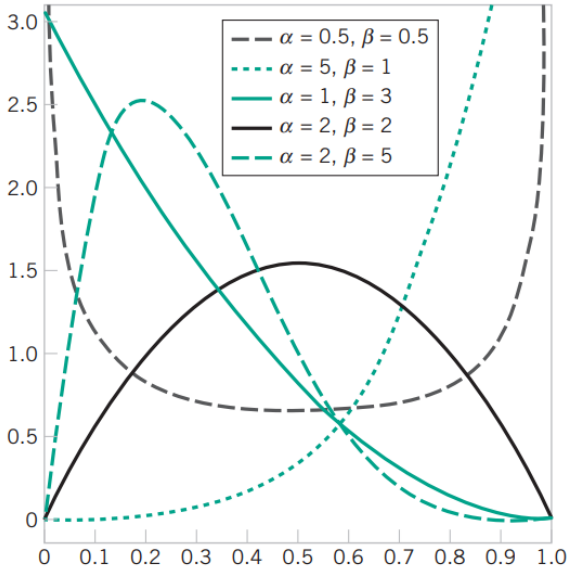

Figure 1. 30 Example of Beta distributions between [0,1] with varying shape factors alpha (α) and beta (β) (Montgomery et al., 2011)

The shapes that mimic the listed distributions (and the reverse of) are ideal for representing distributions of soil properties. However, the Beta distribution can also take on shapes that may not represent the natural characteristics of most geological conditions which are defined within a reasonable limit (i.e. site-specific data, data grouped by general soil type, etc.). An example of an unnatural shaped distribution, with respect to this application of this study, is depicted in Figure 1.30 by the "U-shaped" distribution with α = 0.5 and β = 0.5. The distribution starts to become "U-shaped" if alpha is less than one and beta is less than alpha ($\alpha < 1$ & $\beta < \alpha$).

As the values of the shape parameters increase, the kurtosis increases, and the distribution becomes more leptokurtic (i.e., the distribution becomes thinner and concentrates around the mode.

The Beta distribution can also be defined between defined within a range of minimum (a) and maximum (b) values, commonly referred to as the "Four Parameter Beta Distribution". In this case, the two shape factors can be expressed in terms of the mean, standard deviation, minimum and maximum values (μ, σ, a, b). The shape factors, denoted as alpha (α) and beta (β), must be greater than 0. The beta distribution pdf is expressed by:

$$f\left(y;\alpha,\beta,a,b\right)=\frac{1}{B\left(\alpha,\beta\right)}\left(\frac{y-a}{b-a}\right)^{\alpha-1}\left(\frac{y-x}{b-a}\right)^{\beta-1}\quad for\quad a\le y\le b \tag{1-14}$$

A simple linear relationship exists between a random variable (X) calculated with a Beta distribution within the range [0,1] and a random variable (Y) calculated using the "Four Parameter Beta Distribution" over the range [a, b].

$$Y=a+X\left(b-a\right) \tag{1-15}$$

This linear relationship can be used to shift the mean and variance values between distributions with parameter space. For Beta Distributions of random variable (y) defined within the range [a,b], the mean and variance are expressed in terms of the shape factors alpha and beta:

$$\mu_y=a+\mu_x\left(b-a\right)=a+\frac{\alpha}{\alpha+\beta}\left(b-a\right) \tag{1-16}$$

$$\sigma_y{}^2=\left(b-a\right)^2\sigma_x{}^2=\left(b-a\right)^2\frac{\alpha\beta}{\left(\alpha+\beta\right)^2\left(\alpha+\beta+1\right)} \tag{1-17}$$

The alpha shape parameter can be expressed as,

$$\alpha=\left(\frac{\mu-a}{b-a}\right)\left(\frac{\left(\frac{\mu-a}{b-a}\right)\left(1-\left(\frac{\mu-a}{b-a}\right)\right)}{\frac{\sigma^2}{\left(b-a\right)^2}}-1\right) \tag{1-18}$$

or in terms of CV as:

$$\alpha=\left(\frac{\mu-a}{b-a}\right)\left(\frac{\left(\frac{\mu-a}{b-a}\right)\left(1-\left(\frac{\mu-a}{b-a}\right)\right)}{\frac{\left(CV\mu\right)^2}{\left(b-a\right)^2}}-1\right) \tag{1-19}$$

and the beta shape parameters can be expressed as:

$$\beta=\left(1-\frac{\mu-a}{b-a}\right)\left(\frac{\left(\frac{\mu-a}{b-a}\right)\left(1-\left(\frac{\mu-a}{b-a}\right)\right)}{\frac{\sigma^2}{\left(b-a\right)^2}}-1\right) \tag{1-20}$$

or in terms of CV as:

$$\beta = \left(1 - \frac{\mu - a}{b - a}\right)\left(\frac{\left(\frac{\mu - a}{b - a}\right)\left(1 - \left(\frac{\mu - a}{b - a}\right)\right)}{\frac{\left(CV\mu\right)^2}{\left(b - a\right)^2}} - 1\right) \tag{1-21}$$

Multivariate distributions can be used to represent parameters that are influenced by one another or jointly influenced by separate factors. In the simplest cast, a continues multivariate distribution of two random variables x and y is referred to a bivariate distribution and can be generally represented by $f_{xy}(x, y)$. The influence of parameters on one another is other is referred to as covariance and can be expressed as:

$$Cov[x, y] = E\left[\left(x - \mu_x\right)\left(y - \mu_y\right)\right] \tag{1-22}$$

The covariance depends on the units and variability between two random variables. To obtain information about the strength and direction of a linear relationship, the normalized and nondimensional Pearson correlation coefficient (ρ_{xy}) can be used, which is expressed as:

$$\rho_{xy} = \frac{Cov[x, y]}{\sigma_x \sigma_y} \tag{1-23}$$

The correlation coefficient can range in value from −1 to +1. The sign of the coefficient indicates the direction of the correlation. If both variables tend to increase or decrease together, the coefficient is positive. If one variable tends to increase as the other decreases, the coefficient is negative. The larger the absolute value of the coefficient, the stronger the relationship between the variables. A correlation close to 0 indicates no correlation between the parameters. However, a correlation coefficient near zero does not always mean that no relationship exists between the variables; the variables may have a nonlinear relationship.

The correlation coefficient is also used to express multivariate distributions. Normal distributions are commonly used to represent multivariate because they need only the mean and variance of each parameter to be defined. A continues multivariate normal distribution of two random variables x and y can be expressed as:

$$f_{x,y}(x, y) = \frac{1}{2\pi\sigma_x\sigma_y\sqrt{1 - \rho^2}} e^{\left\{\frac{-1}{2\left(1-\rho^2\right)}\left[\left(\frac{x-\mu_x}{\sigma_x}\right)^2 - 2\rho\frac{\left(x-\mu_x\right)\left(y-\mu_y\right)}{\sigma_x\sigma_y} + \left(\frac{y-\mu_y}{\sigma_y}\right)^2\right]\right\}} \tag{1-24}$$

Probability density functions of bivariate distributions can be represented in a three-dimensional space as depicted in Figure 1.31 or in a two-dimensional space as depicted in **Error! Reference source not found.** 1 .32 which help visualize the effect of the correlation coefficient on the shape of the joint distribution.

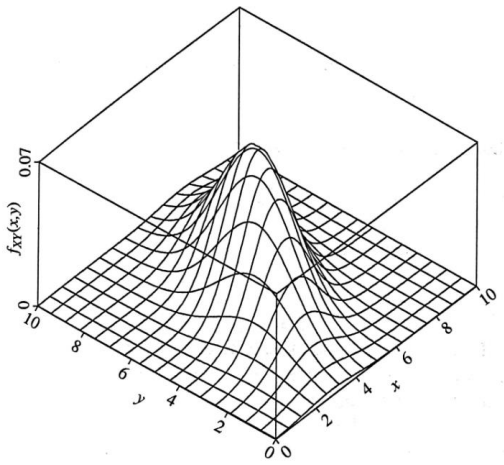

Figure 1.31 Example of bivariate normal probability density function (Fenton and Griffiths, 2008)

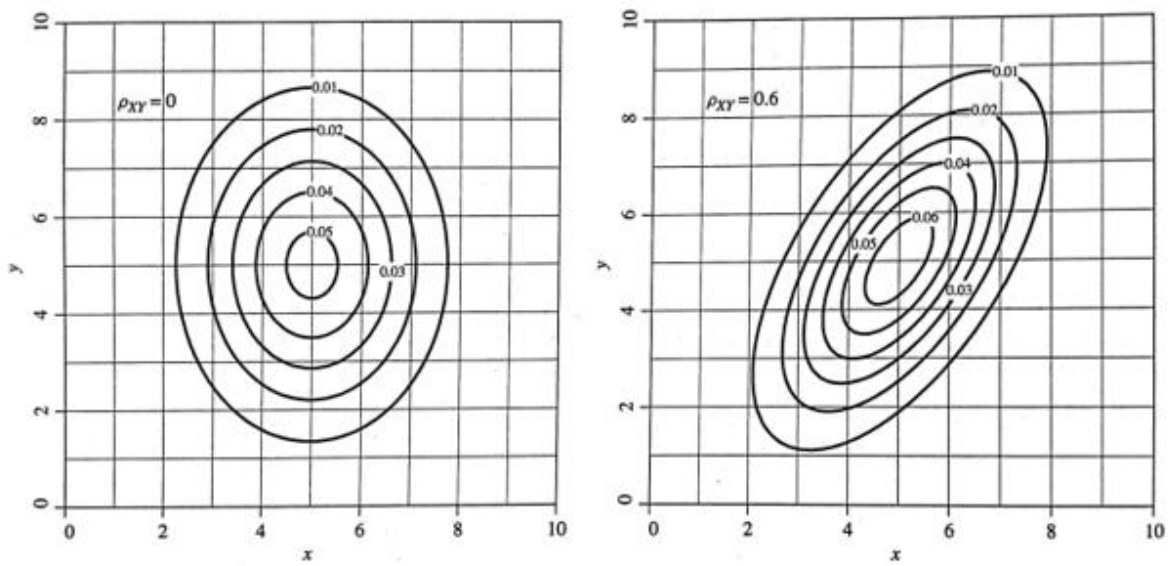

Figure 1.32 Example bivariate probability density functions with $\mu_x = \mu_y = 5$, $\sigma_x = \sigma_y = 1.5$ and correlation coefficients (ρ_{xy}) equal to (a) zero and (b) 0.6 (Fenton and Griffiths, 2008)